Disease Models & Mechanisms 3, 431-440 (2010) doi:10.1242/dmm.002311

RESEARCH ARTICLE

Medaka as a model for human nonalcoholic steatohepatitis

Toshihiko Matsumoto[1], Shuji Terai[1,*], Toshiyuki Oishi[1], Shinya Kuwashiro[1], Koichi Fujisawa[1], Naoki Yamamoto[1], Yusuke Fujita[2], Yoshihiko Hamamoto[2], Makoto Furutani-Seiki[3], Hiroshi Nishina[4] and Isao Sakaida[1]

SUMMARY

The global incidence of nonalcoholic steatohepatitis (NASH) is increasing and current mammalian models of NASH are imperfect. We have developed a NASH model in the ricefish medaka (*Oryzias latipes*), which is based on feeding the fish a high-fat diet (HFD). Medaka that are fed a HFD (HFD-medaka) exhibited hyperlipidemia and hyperglycemia, and histological examination of the liver revealed ballooning degeneration. The expression of lipogenic genes (*SREBP-1c*, *FAS* and *ACC1*) was increased, whereas the expression of lipolytic genes (*PPARA* and *CPT1*) was decreased. With respect to liver fatty acid composition, the concentrations of n-3 polyunsaturated fatty acids (PUFAs) and n-6 PUFAs had declined and the n-3:n-6 ratio was reduced. Treatment of HFD-medaka with the n-3 PUFA eicosapentaenoic acid (EPA) mitigated disease, as judged by the restoration of normal liver fatty acid composition and normal expression levels of lipogenic and lipolytic genes. Moreover, medaka that were fed a diet deficient in n-3 PUFAs developed NASH features. Thus, NASH can be induced in medaka by a HFD, and the proportion of n-3 PUFAs in the liver influences the progress of NASH pathology in these fish. Our model should prove helpful for the dissection of the causes of human NASH and for the design of new and effective therapies.

INTRODUCTION

Nonalcoholic fatty liver disease (NAFLD) is the general term for fatty liver diseases that are not the result of a history of alcohol consumption. NAFLD is the most common cause of human liver dysfunction, and it is estimated that about 30% of the general population in the USA suffers from excessive fat accumulation in the liver (Browning et al., 2004). The incidence of NAFLD, which has been increasing in recent years, is closely tied to obesity, diabetes, hyperlipidemia and insulin resistance. Indeed, NAFLD is considered to be a manifestation of metabolic syndrome in the liver (Powell et al., 1990; Sanyal, 2002). NAFLD can be broadly divided into two subgroups: (1) non-progressive simple steatosis, and (2) nonalcoholic steatohepatitis (NASH) with ballooning degeneration and fibrosis (Schaffner and Thaler, 1986; Younossi et al., 1998; Brunt et al., 1999; Matteoni et al., 1999). In cases of progressive chronic liver disease, NASH may progress from steatohepatitis to liver cirrhosis, and may eventually lead to hepatocellular carcinoma.

There have been many attempts to create NASH models in rodents through the use of either genetic mutation, or dietary or pharmacological manipulation (Anstee and Goldin, 2006). The medaka (*Oryzias latipes*) is a small freshwater fish found in Japan and Asia. This member of the ricefish family has a history of use as an animal model in Japan and a number of purebred strains exist (Masahito et al., 1989). Medaka compare favorably to rodents as experimental animals for drug screening because medaka have a high reproductive rate, mature rapidly, and cost little in terms of rearing space and daily maintenance owing to their small size. Sequencing of the medaka genome has been completed and techniques for producing transgenic and knockout animals have been established (Kasahara et al., 2007; Yamauchi et al., 2000). Physiologically, medaka are omnivores and metabolize sugars and lipids in a manner analogous to that of mammals (Sheridan, 1988; Brown and Tappel, 1959). However, despite their metabolic similarities to humans, medaka have not been used previously for NASH research. In this study, we fed a HFD to medaka to induce NASH and determined whether the progression of liver disease in these fish was similar to the progression of human NASH. In addition, we used our medaka NASH model to verify the efficacy of the administration of the n-3 polyunsaturated fatty acid (PUFA) eicosapentaenoic acid (EPA) as a NASH therapy. Our results have shed much-needed light on the mechanisms potentially underlying NASH in humans, and may point to new avenues of therapy for this debilitating disorder.

RESULTS

Gross anatomical and histopathological evidence for NASH in medaka

For an animal model to be useful for determining the molecular and cellular basis of NASH, it must show the same metabolic abnormalities as the human disease. These anomalies include obesity and insulin resistance; liver damage owing to 'fatty liver' and hyperlipidemia; macrovesicular fat deposition in the liver; infiltration by inflammatory cells; and ballooning degeneration of hepatocytes. Like mammals, medaka have livers, gall bladders, digestive tracts and other internal organs in the peritoneum (Fig. 1A,B). In normal medaka liver tissue, the hepatocytes are arranged

[1]Department of Gastroenterology and Hepatology, Yamaguchi University Graduate School of Medicine, Minami Kogushi 1-1-1, Ube, Yamaguchi 755-8505, Japan
[2]Department of Computer Science and Systems Engineering, Faculty of Engineering, Yamaguchi University, Tokiwadai 2-16-1, Ube, Yamaguchi 755-8505, Japan
[3]Centre for Regenerative Medicine, Department of Biology and Biochemistry, University of Bath, Claverton Down, Bath BA2 7AY, UK
[4]Department of Developmental and Regenerative Biology, Medical Research Institute, Tokyo Medical and Dental University, 1-5-45, Yushima, Bunkyo-ku, Tokyo 113-8510, Japan
*Author for correspondence (terais@yamaguchi-u.ac.jp)

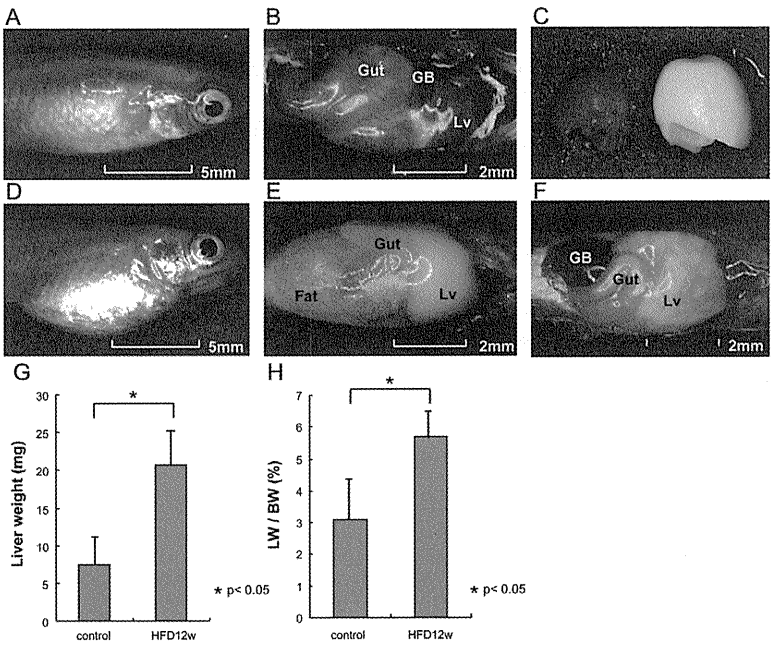

Fig. 1. Altered gross phenotype and liver parameters in HFD-medaka. (A,B) Gross appearance of the abdomen (A) and internal organs (B) of medaka that were fed a control diet for 12 weeks. The abdomen is flat, the liver is brown, and very little visceral fat is observed. Lv, liver; GB, gall bladder; Gut, digestive tract. (C) A comparison of liver color and size in control medaka (left) and HFD-medaka (right). (D,E) Gross appearance of the abdomen (D) and internal organs (E) of medaka that were fed a HFD for 12 weeks. Distention of the abdomen, swelling and whitening of the liver, and a clear increase in visceral fat are seen. (F) Edematous degeneration of the liver in HFD-medaka after 12 weeks. (G,H) Medaka were fed the control diet or the HFD (HFD12w) for 12 weeks, and absolute liver weights (G) and liver weight as a percentage of total body weight (LW/BW) (H), were determined (n=10/group). The results shown in all figure panels are representative of at least three independent trials.

in sheets that are separated by a sinusoidal mesh. Histological examination of normal medaka liver shows that the portal vein, hepatic artery and bile duct are independent, as they are not organized in portal triads (Fig. 2A).

To induce NASH in medaka, 8-week-old fish (n=14/group) were fed either a control diet or a high-fat diet (HFD) for 12 weeks, and monitored for gross anatomical and histological changes at 4, 8 and 12 weeks after HFD initiation. Control medaka grew normally over the 12-week period, from 95±17 mg to 241±32 mg. By contrast, all 14 fish that were fed the HFD exhibited significantly greater body weights, reaching 368±80 mg by the end of the 12 weeks (P<0.05). HFD-medaka also showed distention of the abdomen, owing to increased fat deposition in the viscera, and the presence of a white, swollen liver (Fig. 1C-E). Edematous degeneration of the liver was observed in five out of 14 (36%) HFD-medaka (Fig. 1F). The mean liver weight (Fig. 1G) and the mean liver weight:body weight ratio (Fig. 1H) of HFD-medaka were increased by 2.8-fold and 1.8-fold, respectively, compared with controls, consistent with the observed hepatomegaly in HFD-medaka. Lastly, the weight of intrahepatic total lipids in the HFD-medaka was 6.2-fold greater than in controls (Table 1).

Compared with medaka that were fed a control diet, medaka fed the HFD for 4 weeks exhibited considerably more macrovesicular fat deposition around the hepatic veins (data not shown). By 8 weeks, fat deposition had spread over the entire liver (Fig. 2B; compare with Fig. 2A). By 12 weeks, focal ballooning degeneration and inflammatory cell infiltration in the livers of HFD-medaka were prominent (Fig. 2C,D), consistent with the edematous liver degeneration noted upon gross examination (Fig. 1F). Histopathologically, nine out of 14 (64%) and four out of 14 (29%) HFD-medaka displayed steatohepatitis and simple steatosis, respectively. Liver fibrosis (Fig. 2E,F) and fat accumulation (Fig. 2G) were also observed in these fish. Electron microscopic examination of liver cells from HFD-medaka revealed the presence of lipid droplets (Fig. 2H,I), and the ballooning hepatocytes showed cytoplasmic vacuolation and enlarged lysosomes (Fig. 2H,J).

HFD-medaka show hyperglycemia, hyperlipidemia and altered expression of lipogenic genes

A two-hit theory has been proposed as the mechanism underlying the onset of NASH (Day and James, 1998). The first hit involves increased expression of fatty acid transport-related and lipogenic genes that alter the lipid metabolism inside the liver, such that the liver becomes steatotic. The second hit takes the form of inflammatory cytokines and oxidative stress that drive inflammation and fibrosis. To determine whether a classical first hit was occurring in our HFD-medaka, we analyzed serum components of these fish. Triglyceride (TG) levels in HFD-medaka serum were significantly elevated over those in controls by 4 weeks, and were sevenfold greater by 12 weeks (Fig. 3A). When we analyzed these serum TGs by high-performance liquid chromatography (HPLC), we found that very low-density lipoprotein triglyceride (VLDL-TG) was increased by 15-fold in the serum from HFD-medaka at 12 weeks (2362 mg/dl) compared with controls (160 mg/dl) (Fig. 3B). These results suggested that the HFD-medaka were experiencing an increase in endogenous fatty acid synthesis by hepatocytes. As shown in Fig. 3C, plasma glucose levels were also significantly elevated in HFD-medaka at 8 weeks, and were fourfold greater than in controls by 12 weeks. Serum alanine aminotransferase (ALT) levels were elevated the most (3.7-fold) in HFD-medaka at 4 weeks, but continued to be significantly increased compared with controls at 12 weeks (Fig. 3D). These altered serum parameters parallel our histological examinations of HFD-medaka, in which steatosis was seen at 4 weeks, macrovesicular fat deposition was widespread at 8 weeks, and ballooning degeneration was observed at 12 weeks. Taken together,

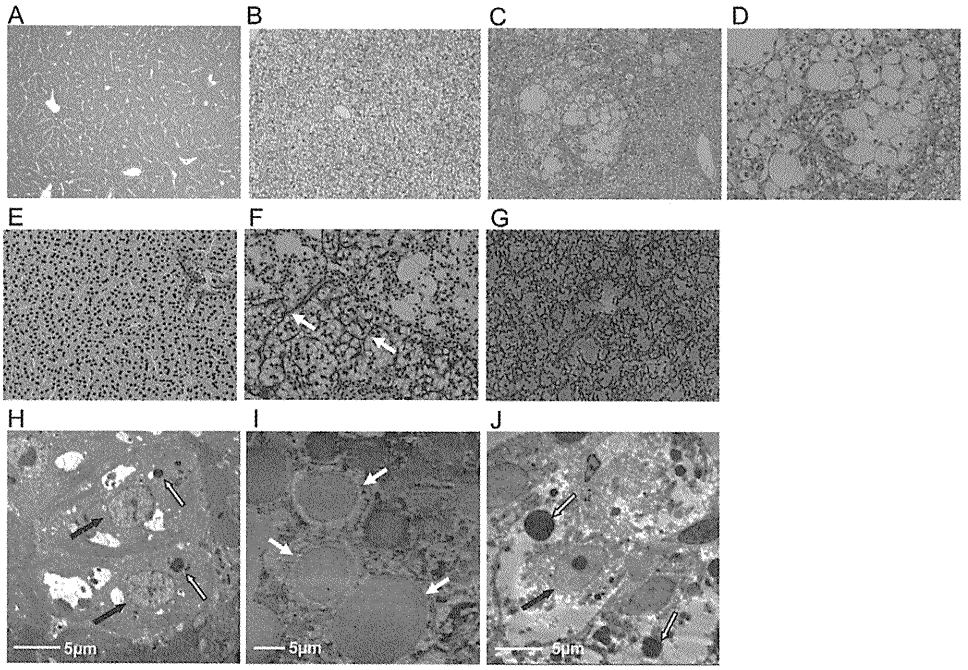

Fig. 2. Altered histopathology in medaka with HFD-induced steatohepatitis. (A) Hematoxylin and eosin (H&E)-stained section of a normal liver from a medaka that was fed the control diet for 12 weeks. The hepatocytes are arranged in sheets separated by a sinusoidal mesh. The portal vein, hepatic artery and bile duct are independent. Magnification ×200. (B) H&E-stained section of a liver from a medaka fed the HFD for 8 weeks. Macrovesicular fat deposition can be seen throughout the entire liver. Magnification ×200. (C,D) H&E-stained section of a liver from HFD-medaka after 12 weeks. In addition to macrovesicular fat deposition, focal ballooning degeneration of hepatocytes accompanied by the infiltration of inflammatory cells can be seen. Magnification ×200 (C); ×400 (D). (E) Gitter staining of the liver from a control medaka at 12 weeks. Magnification ×400. (F) Gitter staining of the liver from a HFD-medaka at 12 weeks. The arrows indicate sinusoidal fibrosis. Magnification ×400. (G) Oil Red O staining of intracellular lipids in the liver of a HFD-medaka at 12 weeks. Magnification ×400. (H) Electron microscopic image of the control medaka in A. Black arrows indicate the nucleus; white arrows indicate the lysosomes. (I) Electron microscopic image of the HFD-fed medaka in B. Arrows indicate hepatocytes loaded with lipid droplets. (J) Electron microscopic image of ballooning degeneration of hepatocytes in the HFD-fed medaka in C. Cytoplasmic vacuolation and enlarged lysosomes can be seen. The black arrow indicates a nucleus; white arrows indicate lysosomes. For A-F, the results shown are representative of 14 medaka examined/group.

these data suggest that a first hit of hyperlipidemia, hyperglycemia and hepatic steatosis occurred in HFD-medaka, followed by a second hit of liver dysfunction owing to ballooning hepatocyte degeneration. Thus, our observations are consistent with the two-hit theory of human NASH development, in which a metabolic abnormality sets the stage for the development of NASH symptoms.

To investigate, at a molecular level, the changes in the fatty acid metabolism of medaka liver during fatty acid loading periods, we used reverse transcription (RT)-PCR to analyze the mRNA expression levels of genes associated with fatty acid synthesis and oxidation. These genes included the main regulator of fatty acid synthesis, sterol regulatory element-binding protein-1c (*SREBP-1c*); the target genes of SREBP-1c, fatty acid synthase (*FAS*) and acetyl-CoA carboxylase 1 (*ACC1*); the main regulator of fatty acid β-oxidation, peroxisome proliferator-activated receptor α (*PPARA*); the mitochondrial β-oxidation marker carnitine palmitoyltransferase 1 (*CPT1*); and the peroxisome β-oxidation marker acyl-CoA oxidase 1 (*ACO1*). Compared with controls, the mRNA expression levels of *SREBP-1c*, *FAS* and *ACC1* were all elevated in HFD-medaka liver at 4 weeks (Fig. 3E, left), confirming that fatty acid synthesis had accelerated in these animals. Conversely, we observed decreased expression of *PPARA* and *CPT1*, but increased expression of *ACO1* (Fig. 3E, right), indicating decreased mitochondrial β-oxidation and accelerated peroxisomal β-oxidation in the HFD-medaka liver. Taken together, these data suggest that HFD-medaka suffer from increased fatty acid synthesis accompanied by decreased fatty acid β-oxidation and inflammation, accounting for their swollen, fatty livers.

To investigate the abnormal fatty acid deposition observed in the HFD-medaka liver, we compared the composition of the fats in control livers with HFD-medaka livers (Table 1). Oleic acid (C18:1n-9) levels in HFD-medaka were clearly higher than in controls, whereas linoleic acid (C18:2n-6), arachidonic acid (C20:4n-6), α-linolenic acid (C18:3n-3), EPA (C20:5n-3) and docosahexaenoic acid (DHA) (C22:6n-3) levels were lower. Although concentrations of both n-3 PUFAs and n-6 PUFAs had declined, the n-3:n-6 ratio was reduced in HFD-medaka because the decrease in n-3 PUFAs was greater than the decrease in n-6 PUFAs. These results are consistent with features of human NASH, in which PUFA levels and n-3:n-6 PUFA ratios are reportedly low in the liver (Araya et al., 2004; Puri et al., 2007). Interestingly, levels of mead acid (C20:3n-9), a marker of essential fatty acid deficiency, were increased in HFD-medaka liver.

Table 1. Fatty acid composition of total lipids in the livers of control, HFD-medaka and HFD+EPA medaka

Fatty acid	Control (molecule %)	HFD (molecule %)	HFD+EPA (molecule %)
C14:0	3.0±0.7	2.1±0.5*	1.4±0.1†
C16:0	26.7±2.1	15.5±2.5*	18.6±2.9†
C18:0	8.7±0.3	2.7±0.9*	3.7±0.6†#
C16:1n-7	4.6±0.4	9.6±0.6*	6.4±0.1†#
C18:1n-9	16.0±1.7	62.5±4.0*	50.4±2.6†#
C20:3n-9	0.2±0.1	1.2±0.3*	0.1±0.1#
C18:2n-6	4.9±0.8	3.9±0.5*	8.4±1.1†#
C18:3n-6	0.5±0.2	1.1±0.4*	1.8±0.1†#
C20:3n-6	0.6±0.4	0.3±0.1	0.1±0.1†#
C20:4n-6	3.0±0.2	1.3±0.4*	0.2±0.1†#
C18:3n-3	0.7±0.2	0.1±0.1*	0.2±0.1†#
C20:5n-3	1.8±0.2	0.1±0.1*	2.1±0.5#
C22:6n-3	23.7±0.7	0.7±0.3*	4.3±1.0†#
Total SFA	38.9±1.6	21.0±3.2*	23.9±3.6†
Total MUFA	22.0±2.1	70.2±3.0*	57.3±2.7†#
Total PUFA	38.9±0.6	7.6±0.2*	18.7±1.1†#
n-3 PUFA	29.5±0.2	0.7±0.3*	8.0±2.0†#
n-6 PUFA	9.4±0.3	6.9±0.3*	10.7±1.0#
n-3:n-6 ratio	3.1±0.1	0.2±0.1*	1.0±0.1†#
Total lipid (mg/g of tissue)	27±9	167±62*	87±28†#

All values are means (molecule %) ± S.E.M. SFA, saturated fatty acid; MUFA, monounsaturated fatty acid; PUFA, polyunsaturated fatty acid. n=6/group; *P<0.05 versus control, †P<0.05 versus control, #P<0.05 versus HFD.

EPA treatment inhibits NASH development in medaka

Because administration of the n-3 PUFA EPA has been investigated as a therapy for human NASH, we explored whether EPA treatment could slow disease progression in our medaka NASH model. Medaka were fed a HFD with or without EPA for 12 weeks. The HFD+EPA medaka showed increased fat deposition in the internal organs and a white, swollen liver similar to that observed in the HFD group (Fig. 4A). However, histological examination revealed that the degree of fat deposition in the HFD+EPA group appeared to be less than that in the HFD group during the same period (Fig. 4B). Indeed, analysis of total lipids showed that the fat levels in the HFD+EPA liver were 48% lower than in the HFD liver (Table 1). Moreover, unlike HFD-medaka, the HFD+EPA medaka were not hyperglycemic after fasting (Fig. 4C). HLPC analysis showed that serum TG and VLDL-TG levels were 16% (3132 vs 2643 mg/dl) and 21% (2362 vs 1873 mg/dl) lower in HFD+EPA livers compared with HFD livers, respectively (Fig. 4D). EPA treatment increased EPA (C20:5n-3) and DHA (C22:6n-3) levels, as well as the n-3:n-6 PUFA ratio, in the liver (Table 1). Finally, mead acid (C20:3n-9) levels were decreased in HFD+EPA livers compared with HFD livers (Table 1), suggesting that any essential fatty acid deficiencies that were present had been mitigated.

With respect to gene expression, the levels of *SREBP-1c*, *FAS* and *ACC1* mRNAs were reduced in HFD+EPA medaka compared with HFD-medaka, and the accelerated fatty acid synthesis caused by HFD consumption was abrogated (Fig. 4E, top). By contrast, the levels of *PPARA* and *CPT1* expression were increased, *ACO1* expression was decreased, and markers of mitochondrial β-oxidation became predominant in the HFD+EPA liver (Fig. 4E, bottom). Thus, the pattern of gene expression in livers of HFD+EPA medaka was essentially the same as that in medaka fed the control diet. These data indicate that de novo fatty acid synthesis in HFD-medaka liver decreases upon EPA treatment, and that normal fat utilization is restored.

n-3 PUFA deficiency induces NASH

It has been reported that liver PUFA levels and n-3:n-6 PUFA ratios are low in NASH patients (Araya et al., 2004; Puri et al., 2007). We therefore investigated whether a deficiency in n-3 PUFA could induce NASH in medaka. We prepared an n-3 PUFA-deficient (n-3PUFA$^-$) diet with about the same energy content as the control diet, and used it to feed medaka for 8 weeks. Compared with controls, the n-3PUFA$^-$ medaka showed moderate increases in fat deposition in internal organs, and their livers, although pink, were swollen (Fig. 5A). By gross observation, five out of ten (50%) n-3PUFA$^-$ medaka showed edematous degeneration of the liver, and histopathological examination revealed that steatohepatitis was present in seven out of ten (70%) of these animals (Fig. 5B). The mean serum ALT value in n-3PUFA$^-$ medaka was 442±228 IU/l (Fig. 5C), confirming the presence of liver damage. Thus, NASH is induced in medaka by conditions of n-3PUFA deficiency.

DISCUSSION

Medaka compare favorably to rodents as experimental animals for drug screening because medaka have a high reproductive rate, mature rapidly, and cost little in terms of rearing space and daily maintenance owing to their small size. Our results show that NASH can be induced in medaka by feeding a HFD, and that the development of NASH can be largely prevented by EPA administration. Importantly, we have also demonstrated that n-3 PUFA deficiency can induce NASH in medaka.

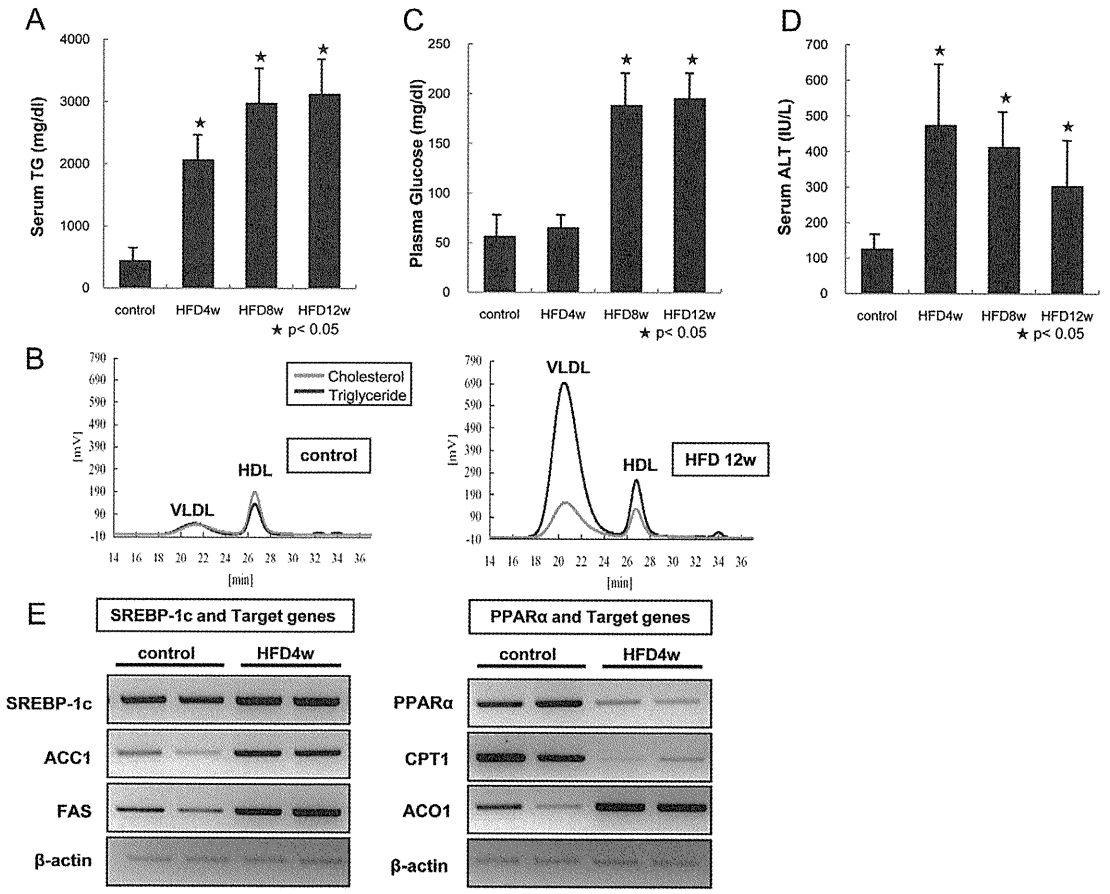

Fig. 3. HFD induces hyperglycemia, hyperlipidemia and the expression of lipogenic genes. (A) Increased TGs. After 12 hours of fasting, serum TG levels were measured in control and HFD-medaka at 4, 8 and 12 weeks. A significant elevation in serum TGs in HFD-medaka was seen by as early as 4 weeks on a HFD (n=10/group). (B) Increased VLDL and high-density lipoprotein (HDL). Serum samples from control (left) and HFD-medaka (right) at 12 weeks were fractionated by HPLC to detect cholesterol and TG levels (n=10/group). A 15-fold increase in serum VLDL-TG was observed in HFD-medaka compared with controls. (C) Increased fasting blood sugar. Plasma glucose was measured in the medaka in A after 12 hours of fasting. Plasma glucose was fourfold higher in the HFD-medaka liver than in controls at 12 weeks (n=12/group). (D) Increased ALT. Serum ALT was measured in the medaka in A and was found to be elevated most highly after 4 weeks on a HFD (n=10/group). (E) Altered expression of lipogenic (left) and lipolytic (right) genes. mRNA levels of the indicated genes in livers from control and HFD-medaka at 4 weeks were determined by semi-quantitative RT-PCR. *SREBP-1c*, *ACC1* and *FAS* were all elevated in HFD-medaka compared with control medaka. Conversely, the mRNA levels of *PPARA* and *CPT1* were reduced and *ACO1* was increased (n=6/group).

We were able to induce steatohepatitis in medaka through feeding, thus creating a NASH model that is easily established in a relatively short period of time. The features of our model include the efficient induction of ballooning degeneration, a key feature in the diagnosis of human NASH (Brunt et al., 1999; Matteoni et al., 1999; Neuschwander-Tetri and Caldwell, 2003). The frequency of ballooning degeneration in normal medaka is 10-20% (Bunton, 1990; Boorman et al., 1997; Brown-Peterson et al., 1999), whereas our HFD-medaka showed a ballooning degeneration frequency of greater than 60%. By contrast, Deng et al. have shown that 46% of C57BL/6 mice fed a HFD through an implanted gastrostomy tube develop steatohepatitis (Deng et al., 2005). Thus, our medaka model of NASH induction is slightly superior to the mouse model in terms of the efficiency of ballooning degeneration induction (64% vs 46%).

The mechanisms underlying the digestion and absorption of lipids; the transport of exogenous and endogenous lipids; and fatty acid oxidation are almost identical in fish and mammals (Brown and Tappel, 1959; Sheridan, 1988). However, there are some differences in how fatty acids are released from intestinal epithelial cells into blood vessels or lymph ducts (Sheridan, 1988). In mammals, short chain fatty acids (SCFAs) and medium chain fatty acids (MCFAs) that are absorbed by intestinal epithelial cells are released directly into the portal vein without esterification. Most long chain fatty acids (LCFAs) are resynthesized into TGs and released into lymph ducts as chylomicron particles, but some are released into the portal vein without esterification. In fish, LCFAs are rapidly processed into free fatty acids (FFAs), and only later are resynthesized as TGs and released as chylomicron

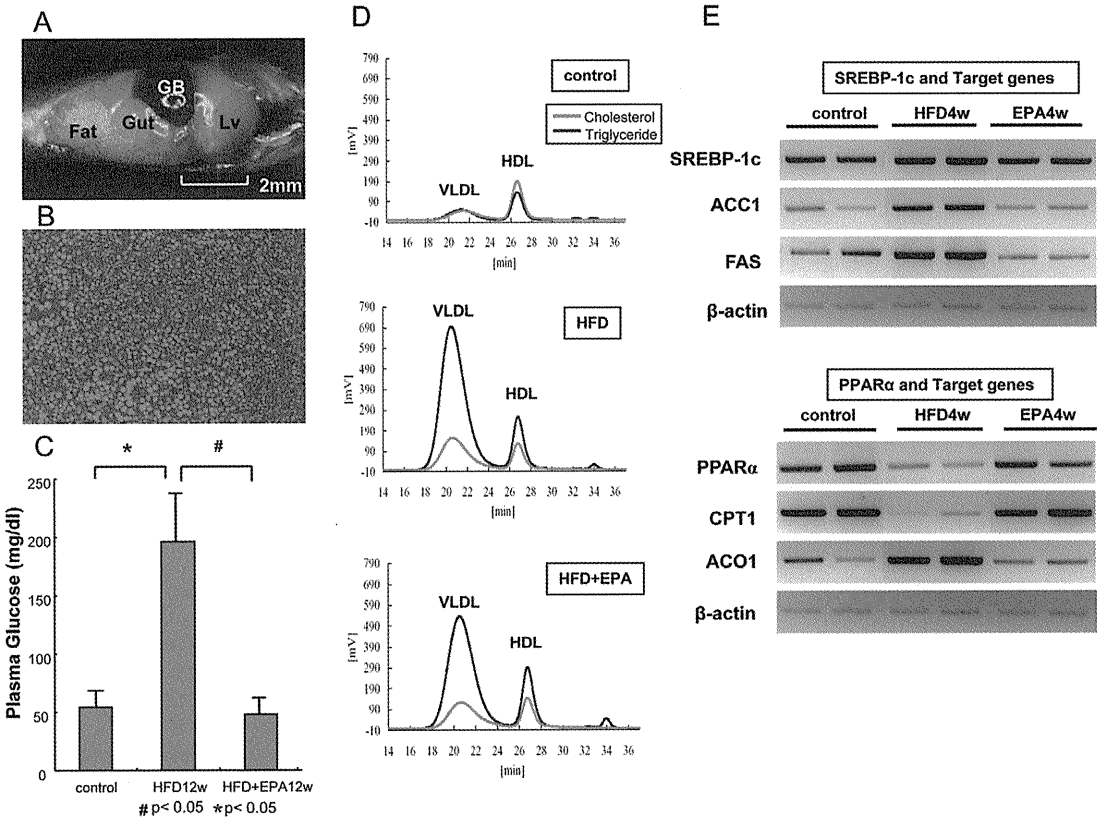

Fig. 4. EPA treatment inhibits NASH development in medaka. (A) Gross appearance of the abdomen from an HFD+EPA medaka. A white, swollen liver and increased visceral fat are visible in the HFD+EPA medaka after 12 weeks on a HFD. (B) Ameliorated histopathology. An H&E-stained section of a liver from an HFD+EPA medaka at 12 weeks. Macrovesicular fat deposition can be seen but there is very little ballooning degeneration. (C) Normal fasting blood sugar. After 12 hours of fasting, the plasma glucose level of HFD+EPA medaka at 12 weeks was the same as that in controls. The hyperglycemia that was evident in HFD-medaka at 12 weeks was not observed. (D) Decreased TG. Serum samples from control, HFD-medaka and HFD+EPA medaka at 12 weeks were analyzed by HPLC as for Fig. 3B. HFD+EPA medaka showed a 21% decrease in serum VLDL-TG compared with HFD-medaka. For A-D, the results shown are representative of 10-12 individuals that were examined/group. (E) Restored gene expression. mRNA levels of the indicated lipogenic and lipolytic genes were examined in control, HFD-medaka and HFD+EPA medaka at 4 weeks by semi-quantitative RT-PCR as for Fig. 3E. Compared with HFD-medaka, the mRNA levels of *SREBP-1c*, *ACC1* and *FAS* were reduced in HFD+EPA medaka and resembled those in medaka that were fed the control diet. Conversely, the expression levels of *PPARA* and *CPT1* were increased in HFD+EPA medaka, whereas the level of *ACO1* was decreased. This pattern also resembled that observed in medaka that were fed the control diet (n=6/group).

particles into the blood (Robinson and Mead, 1973; Sheridan, 1988). Our medaka NASH model was created by feeding a HFD based on LCFAs, and we believe that many of the consumed LCFAs arrive in the liver as FFA-albumin complexes. In obese humans that develop NASH, insulin signaling in adipocytes is disrupted such that hormone-sensitive lipases hydrolyze TGs into fatty acids (Hotamisligil et al., 1995). These fatty acids are subsequently released from the adipocytes and enter the liver through the portal vein, exacerbating NASH development (Hotamisligil et al., 1995; Day, 2002). We believe that a similar scenario occurs in our HFD-medaka, such that FFAs derived from consumed LCFAs flow into the liver. After obesity develops in medaka, FFAs from fat tissues may also join this flow, perhaps explaining why NASH develops more easily in medaka than in other animal models.

In contrast to the lipids of terrestrial vertebrates, fish lipids contain a high proportion of PUFAs, particularly the n-3 PUFAs whose function is to maintain lipid liquidity at low temperature. However, as with terrestrial mammals, fish are unable to synthesize n-6 and n-3 PUFAs, making these molecules essential fatty acids that must be consumed. The HFD used in our study included 64.9% oleic acid, 12.8% palmitic acid (C16:0), 7.6% stearic acid (C18:0), 10.3% linoleic acid and 0.2% α-linolenic acid. Monounsaturated fatty acids (MUFAs) and saturated fatty acids (SFAs) accounted for most of the fatty acids, with only an extremely small proportion of α-linolenic acid being present. The synthesis of highly unsaturated fatty acids (HUFAs), such as arachidonic acid, EPA, DHA and other fatty acids with a carbon chain length of greater than 20, depends on the action of delta-6 and delta-5 desaturases (Sprecher, 1981). These enzymes preferentially desaturate n-3PUFAs then n-6PUFAs

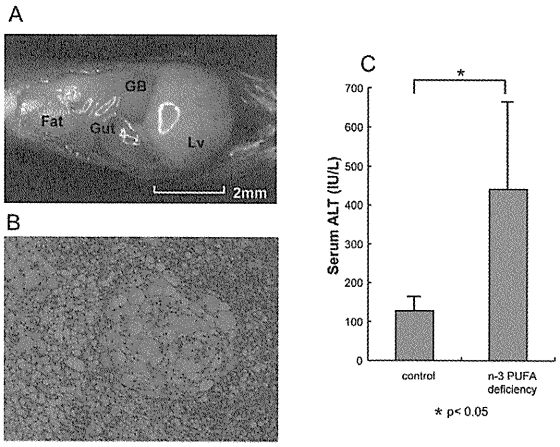

Fig. 5. n-3 PUFA deficiency induces NASH in medaka. (A) Gross appearance of the abdomen. Edematous degeneration accompanying liver swelling and a slight increase in visceral fat is observed in medaka fed an n-3 PUFA-deficient (n-3PUFA$^-$) diet for 8 weeks. (B) An H&E-stained section of liver from an n-3 PUFA$^-$ medaka. Macrovesicular fat deposition is visible throughout the liver, as is focal ballooning degeneration. For A and B, the results shown are representative of ten individuals that were examined/group. (C) Serum ALT values of the n-3 PUFA$^-$ medaka in A and B were twofold to fourfold higher than those in medaka that were fed the control diet (n=10/group).

Table 2. Composition of control, HFD and n-3 PUFA-deficient diets

Diet	Grams/100 g	Calorie %	Kcal/100 g
Control diet			
Protein	50.0	62.5	200.0
Fat	9.0	25.3	81.0
Carbohydrates	11.0	13.8	44.0
Total			325.0
n-3 PUFA-deficient diet			
Protein	21.5	23.9	86.0
Fat	4.4	11.0	39.6
Carbohydrates	58.6	65.1	234.4
Total			360.0
HFD diet			
Protein	25.5	20.1	102.0
Fat	32.0	56.7	288.0
Carbohydrates	29.4	23.2	117.6
Total			507.6

and then n-9PUFAs in a process that is controlled by HUFAs (Cho et al., 1999). Thus, EPA and DHA levels and n-3:n-6 PUFA ratios declined in our HFD-medaka owing to their greatly reduced consumption of α-linolenic acid, EPA and DHA. By contrast, the levels of mead acid increased in HFD-medaka owing to the desaturation of oleic acid. In HFD-medaka treated with EPA, the increased levels of EPA and DHA in the liver probably inhibited the activity of delta-6 and delta-5 desaturases. As a result, the conversion of linoleic acid to arachidonic acid, as well as that of oleic acid to mead acid, was inhibited.

The n-3 PUFAs are ligands for PPARα, and PPARα activation increases the expression of fatty acid oxidation enzymes such that fatty acid oxidation is promoted (Gottlicher et al., 1992; Forman et al., 1997; Ren et al., 1997). Therefore, when PUFAs are deficient, fatty acid oxidation declines and livers accumulate fat (Fukazawa et al., 1971). In our medaka NASH model, expression of the mRNA encoding the lipogenic transcription factor SREBP-1c was induced, and expression levels of the fatty acid synthesis pathway enzymes ACC1 and FAS were increased. Conversely, expression levels of the lipolytic transcription factor PPARα, as well as those of CPT1 (the rate-limiting enzyme in mitochondrial β-oxidation), were reduced. Concomitantly, the expression of ACO1, which is involved in peroxisome β-oxidation, was increased. The observed reduction in CPT1 expression may be attributable to the production of malonyl CoA, an intermediate product of fatty acid synthesis. Malonyl CoA interferes with CPT1 expression, and it is thought that compensatory peroxisome β-oxidation is induced (McGarry et al., 1977).

In humans, n-3 PUFA deficiency has been linked to neuropathy and immune system impairment (Holman, 1998). Variations in n-3 PUFA concentrations in the liver may thus indirectly regulate the inflammation associated with NASH. The notion that n-3 PUFAs are involved in the pathology seen in our medaka NASH model is supported by the observation that the expression levels of genes involved in fatty acid metabolism were restored to control levels when HFD-medaka were treated with EPA.

In conclusion, our study shows that the induction of fatty liver and the reproduction of NASH pathology in medaka can be achieved by feeding a diet that is low in EPA and DHA, but that has about the same energy content as a control diet. Moreover, our model is easily, cheaply and rapidly established in the laboratory, allowing ample latitude for exploration of its usefulness. We anticipate that our medaka NASH model will indeed be helpful for clarifying human NASH pathology and for assisting in the development of novel therapeutics aimed at preventing or alleviating this burgeoning health problem.

METHODS

Animals

Himedaka strain Cab (an orange-red variety of medaka, *Oryzias latipes*) fish that were 8 weeks old were used for most experiments. Fish were maintained at a stocking level of ten fish/tank in tap water with aeration. The ten fish in a given tank received a daily ration of 200 mg of the diet prescribed for that group, an amount that was consumed completely within 14 hours. All fish were maintained in accordance with the Animal Care Guidelines of Yamaguchi University. During experiments, fish were kept in plastic tanks covered with plastic covers and illuminated with fluorescent light from 8:00 a.m. to 10:00 p.m. The tank water temperature was maintained at 26±1°C.

Diets

The proportions of protein, fat and carbohydrate, as well as the fatty acid compositions, of the control, HFD and n-3 PUFA-deficient diets that were used in this study are shown in Tables 2 and 3. The energy content of the control diet (Hikari Crest; Kyorin Co. Ltd, Hyogo, Japan) was 3.3 kcal/g, with 25.3% of the calories

Table 3. Fatty acid composition of control, HFD and n-3 PUFA-deficient diets

Fatty acid		Control (g/100 g)	HFD (g/100 g)	n-3 PUFA deficiency (g/100 g)
Myristic acid	C14:0	0.42	0.35	0.02
Myristoleic acid	C14:1n-5	0.00	0.10	0.00
Pentadecanic acid	C15:0	0.00	0.03	0.00
Palmitic acid	C16:0	2.11	4.03	0.66
Palmitoleic acid	C16:1n-7	0.50	0.38	0.01
Heptadecanic acid	C17:0	0.00	0.13	0.00
Heptadecenic acid	C17:1	0.00	0.10	0.01
Stearic acid	C18:0	1.03	2.40	0.22
Oleic acid	C18:1n-9	1.38	20.50	0.92
Linoleic acid	C18:2n-6	0.88	3.26	2.31
α-Linolenic acid	C18:3n-3	0.13	0.06	0.22
Arachidic acid	C20:0	0.02	0.10	0.01
Gondoic acid	C20:1n-9	0.19	0.10	0.03
Arachidonic acid	C20:4n-6	0.08	0.00	0.00
Eicosapentaenoic acid	C20:5n-3	0.93	0.00	0.00
Behenic acid	C22:0	0.00	0.06	0.01
Erucic acid	C22:1n-9	0.03	0.00	0.00
Docosapentaenoic acid	C22:5n-3	0.13	0.00	0.00
Lignoceric acid	C24:0	0.02	0.00	0.00
Docosahexaenoic acid	C22:6n-3	1.07	0.00	0.00
Nervonic acid	C24:1n-9	0.04	0.00	0.00
Total (g/100 g)		8.96	31.60	4.42
Total PUFA (g/100 g)		3.22	3.32	2.53
n-3 PUFA (g/100 g)		2.26	0.06	0.22
n-6 PUFA (g/100 g)		0.96	3.26	2.31
n-3:n-6 ratio		2.35	0.02	0.10

from fat, 62.5% of calories from protein, and 13.8% of calories from carbohydrate, plus vitamins and minerals as recommended. The energy content of the high-fat diet (HFD32; CLEA Japan Inc., Tokyo, Japan) was 5.1 kcal/g, with 56.7% of calories from fat, 20.1% of calories from protein, and 23.2% of calories from carbohydrate, plus vitamins and minerals as recommended. The n-3 PUFA-deficient (EPA- and DHA-deficient) diet, which consisted of fish meal-free powder (F1 diet; Funabashi Farm Co. Ltd, Chiba, Japan), had an energy content of 3.6 kcal/g, with 11.0% of calories from fat, 23.9% of calories from protein, and 65.1% of calories from carbohydrate, plus vitamins and minerals as recommended. For EPA treatment, eicosapentaenoic acid ethyl ester (EPA-E, purity >99%; Mochida Pharmaceutical Co. Ltd, Tokyo, Japan) was mixed with HFD32 to a concentration of 5% by weight.

Histology

Euthanized fish were slit open from the anal vent to the gills, and the entire body was fixed with 4% paraformaldehyde in 0.1 M phosphate buffer (Muto, Tokyo, Japan). The liver was dissected, dehydrated in alcohol, and embedded in paraffin according to standard procedures. Serial sections (3-5 μm thick) were cut and stained with hematoxylin and eosin (H&E). Liver fibrosis was assessed by Gitter staining. Intracellular lipids were stained with Oil Red O to analyze fat accumulation in the liver.

Electron microscopy

Chunks of medaka liver were fixed with 2% glutaraldehyde and 4% paraformaldehyde in 0.1 M phosphate buffer for 30 minutes at 4°C. Fixed liver pieces were washed thoroughly in 0.1 M phosphate buffer, post-fixed for 30 minutes with 1% osmium tetraoxide in 0.1 M phosphate buffer, and then block-stained with 2% aqueous uranyl acetate for 30 minutes to enhance the contrast for electron microscopy. Samples were dehydrated through a graded ethanol series, infused with propylene oxide, and embedded in epoxy resin. Ultra-thin sections were collected on copper grids, stained with 2% aqueous uranyl acetate for 8 minutes and 0.5% lead citrate for 8 minutes, followed by examination under a Hitachi H7500 electron microscope.

Blood analysis

Blood samples were obtained from medaka following a 12-hour fast. Fish were kept on ice for 1-2 minutes and then bled by cutting a ventral portion of the tail fin. Blood was collected in a microcapillary tube and the volume measured. Blood samples were kept at room temperature for 1 hour before centrifugation at 1200 × *g* for 30 minutes at 4°C. Serum ALT concentrations were measured using a Fuji Dry-Chem 3500 (Fuji Film Co. Ltd, Tokyo, Japan). Plasma glucose levels were determined using a Glucocard G-meter (Arkray Co. Ltd, Kyoto, Japan). Cholesterol and TG

Table 4. Primers for seven genes examined in the livers of HFD-medaka

Gene	Forward primer (5′ to 3′)	Reverse primer (3′ to 5′)
ACC1	GAGTGACGTCCTGCTTGACA	ACCTTTGGTCCACCTCACAG
ACO1	GCTCAGCTTTACAGCCTTGG	GGACGATTCCCTAACGATCA
CPT1	ATGTCTACCTCCGTGGACGA	CAAGTTTGGCCTCTCCTTTG
FAS	GACGCTTCAGGAAATGGGTA	GGACAGGAACCGGACTATCA
PPARA	TCTTGAGTGTCGGGTGTGTG	CGGTAGAGCCCACCATCTT
SREBP-1c	CCCAACCAGATGAGGAGAAA	AGGACTTTTGTGCTGCTCGT
β-actin	CTGGACTTCGAGCAGGAGAT	GCTGGAAGGTGGACAGAGAG

profiles in total lipoproteins were analyzed using a dual-detection HPLC system (Skylight Biotech, Akita, Japan) with two tandem-connected TSKgel LipopropakXL columns (300 × 7.8 mm; Tosoh, Japan).

Fatty acid analysis

The fatty acid composition of homogenized liver tissue (20 mg tissue/ml saline) was determined by capillary gas chromatography. Total lipids were extracted by Folch's procedure (Folch et al., 1957), and fatty acids were methylated with boron trifluoride and methanol. Methylated fatty acids were analyzed using a Shimadzu GC-17A gas chromatograph (Shimadzu Co. Ltd, Kyoto, Japan) and a BPX70 capillary column (0.25 mm internal diameter × 30 mm; SGE International Ltd, Melbourne, Australia). Tricosanoic acid (C23:0) was used as the internal standard. The minimum detectable fatty acid concentration detected by this assay is 0.5 μg/ml.

Semi-quantitative RT-PCR

To avoid any acute effects of food intake, fish were fasted overnight prior to sacrifice. Livers were isolated and total RNA was extracted and purified using the RNeasy kit (Qiagen, Hilden, Germany). cDNAs were synthesized using purified RNA plus random hexamers and the Transcriptor First Strand cDNA synthesis kit (Roche, Indianapolis, IN). Semi-quantitative RT-PCR was performed using a PCR master mix (Promega, Madison, WI) and the primers listed in Table 4. Gene expression levels were normalized against β-actin (endogenous control).

Statistical analyses

Numerical data are expressed as the mean ± S.D. The Student's *t*-test was performed to assess statistical significance among groups of medaka. *P* values less than 0.05 were considered to be significant.

ACKNOWLEDGEMENTS

This study was supported by Grants-in-Aid for Scientific Research from the Japan Society for the Promotion of Science (Nos. 18590737, 18659209, 19590693, 19390199, 20659116 and 21659189); the Knowledge Cluster Initiative; the Ministry of Health, Labour and Welfare; and Japan Aerospace Exploration Agency (JAXA). We also thank Dr Masaaki Soma and Dr David Tosh for critical reading of the manuscript.

COMPETING INTERESTS

The authors declare no competing financial interests.

AUTHOR CONTRIBUTIONS

T.M., S.T. and I.S. conceived and designed the experiments; T.M., S.K., K.F., T.O. and N.Y. performed the experiments; T.M., Y.F. and Y.H. analyzed the data; M.F.-S. and H.N. contributed reagents, materials and analytical tools; T.M. and S.T. wrote the paper.

Received 25 November 2008; Accepted 29 October 2009.

TRANSLATIONAL IMPACT

Clinical issue

Nonalcoholic fatty liver disease (NAFLD) is the most common cause of human liver dysfunction, and an estimated 30% of the general population of the USA suffer from excessive fat accumulation in the liver. NAFLD is broadly divided into two subgroups: (1) non-progressive simple steatosis, and (2) nonalcoholic steatohepatitis (NASH) with worsening degeneration and fibrosis. In cases of progressive chronic liver disease, NASH may progress from steatohepatitis to liver cirrhosis, and may eventually lead to hepatocellular carcinoma. A lack of knowledge about the mechanisms that lead to NASH progression prevent advances in drug development.

Results

The authors establish a NASH model using the ricefish medaka (*Oryzias latipes*), which were fed a high-fat diet (HFD) for 12 weeks (HFD-medaka). HFD-medaka exhibited hyperlipidemia, hyperglycemia and hepatic steatosis, with progressive hepatocyte degeneration that led to liver dysfunction. These findings are consistent with NASH progression in humans.

Expected genetic changes were also detected in the NASH model, including increased expression of lipogenic genes and decreased expression of lipolytic genes after HFD feeding. The concentrations of n-3 polyunsaturated fatty acids (PUFAs) and n-6 PUFAs declined, and the n-3:n-6 ratio was reduced in HFD-fed animals, which reflects the biochemistry in humans. Treating HFD-fed medaka with a drug used to treat human NASH [n-3 PUFA eicosapentaenoic acid (EPA)] mitigated disease, restoring normal liver fatty acid composition and normal expression levels of lipogenic and lipolytic genes. Moreover, medaka that were fed a diet deficient in n-3 PUFAs developed features of NASH. This NASH model demonstrates that the proportion of n-3 PUFAs that are present in the liver plays an important role in the progress of NASH pathology.

Implications and future directions

The medaka genome was recently sequenced, making it amenable to forward genetic screens with N-ethyl-N-nitrosourea (ENU), and morpholino knockdown. These techniques promote the analysis of specific gene mutations in these fish. Thus, with their high reproductive rate, rapid maturation and low maintenance costs, medaka compare favorably with rodents as experimental animals. This NASH model is a useful tool to study the unknown mechanisms underlying human liver disease, and should eventually be useful for therapeutic screen tests.

doi:10.1242/dmm.005355

REFERENCES

Anstee, Q. M. and Goldin, R. D. (2006). Mouse models in non-alcoholic fatty liver disease and steatohepatitis research. *Int. J. Exp. Pathol.* **87**, 1-16.

Araya, J., Rodrigo, R., Videla, L. A., Thielemann, L., Orellana, M., Pettinelli, P. and Poniachik, J. (2004). Increase in long-chain polyunsaturated fatty acid n-6/n-3 ratio in relation to hepatic steatosis in patients with non-alcoholic fatty liver disease. *Clin. Sci. (Lond.)* **106**, 635-643.

Boorman, G. A., Botts, S., Bunton, T. E., Fournie, J. W., Harshbarger, J. C., Hawkins, W. E., Hinton, D. E., Jokinen, M. P., Okihiro, M. S. and Wolfe, M. J. (1997). Diagnostic criteria for degenerative, inflammatory, proliferative nonneoplastic and neoplastic liver lesions in medaka (Oryzias latipes): consensus of a National Toxicology Program Pathology Working Group. *Toxicol. Pathol.* **25**, 202-210.

Brown, W. D. and Tappel, A. L. (1959). Fatty acid oxidation by carp liver mitochondria. *Arch. Biochem. Biophys.* **85**, 149-158.

Brown-Peterson, N. J., Krol, R. M., Zhu, Y. and Hawkins, W. E. (1999). N-nitrosodiethylamine initiation of carcinogenesis in Japanese medaka (Oryzias latipes): hepatocellular proliferation, toxicity, and neoplastic lesions resulting from short term, low level exposure. *Toxicol. Sci.* **50**, 186-194.

Browning, J. D., Szczepaniak, L. S., Dobbins, R., Nuremberg, P., Horton, J. D., Cohen, J. C., Grundy, S. M. and Hobbs, H. H. (2004). Prevalence of hepatic steatosis in an urban population in the United States: impact of ethnicity. *Hepatology* **40**, 1387-1395.

Brunt, E. M., Janney, C. G., Di Bisceglie, A. M., Neuschwander-Tetri, B. A. and Bacon, B. R. (1999). Nonalcoholic steatohepatitis: a proposal for grading and staging the histological lesions. *Am. J. Gastroenterol.* **94**, 2467-2474.

Bunton, T. E. (1990). Hepatopathology of diethylnitrosamine in the medaka (Oryzias latipes) following short-term exposure. *Toxicol. Pathol.* **18**, 313-323.
Cho, H. P., Nakamura, M. T. and Clarke, S. D. (1999). Cloning, expression, and nutritional regulation of the mammalian Delta-6 desaturase. *J. Biol. Chem.* **274**, 471-477.
Day, C. P. (2002). Pathogenesis of steatohepatitis. *Best Pract. Res. Clin. Gastroenterol.* **16**, 663-678.
Day, C. P. and James, O. F. (1998). Steatohepatitis: a tale of two "hits"? *Gastroenterology* **114**, 842-845.
Deng, Q. G., She, H., Cheng, J. H., French, S. W., Koop, D. R., Xiong, S. and Tsukamoto, H. (2005). Steatohepatitis induced by intragastric overfeeding in mice. *Hepatology* **42**, 905-914.
Folch, J., Lees, M. and Sloane Stanley, G. H. (1957). A simple method for the isolation and purification of total lipides from animal tissues. *J. Biol. Chem.* **226**, 497-509.
Forman, B. M., Chen, J. and Evans, R. M. (1997). Hypolipidemic drugs, polyunsaturated fatty acids, and eicosanoids are ligands for peroxisome proliferator-activated receptors alpha and delta. *Proc. Natl. Acad. Sci. USA* **94**, 4312-4317.
Fukazawa, T., Privett, O. S. and Takahashi, Y. (1971). Effect of EFA deficiency on lipid transport from liver. *Lipids* **6**, 388-393.
Gottlicher, M., Widmark, E., Li, Q. and Gustafsson, J. A. (1992). Fatty acids activate a chimera of the clofibric acid-activated receptor and the glucocorticoid receptor. *Proc. Natl. Acad. Sci. USA* **89**, 4653-4657.
Holman, R. T. (1998). The slow discovery of the importance of omega 3 essential fatty acids in human health. *J. Nutr.* **128**, 427S-433S.
Hotamisligil, G. S., Arner, P., Caro, J. F., Atkinson, R. L. and Spiegelman, B. M. (1995). Increased adipose tissue expression of tumor necrosis factor-alpha in human obesity and insulin resistance. *J. Clin. Invest.* **95**, 2409-2415.
Kasahara, M., Naruse, K., Sasaki, S., Nakatani, Y., Qu, W., Ahsan, B., Yamada, T., Nagayasu, Y., Doi, K., Kasai, Y. et al. (2007). The medaka draft genome and insights into vertebrate genome evolution. *Nature* **447**, 714-719.
Masahito, P., Aoki, K., Egami, N., Ishikawa, T. and Sugano, H. (1989). Life-span studies on spontaneous tumor development in the medaka (Oryzias latipes). *Jpn. J. Cancer Res.* **80**, 1058-1065.
Matteoni, C. A., Younossi, Z. M., Gramlich, T., Boparai, N., Liu, Y. C. and McCullough, A. J. (1999). Nonalcoholic fatty liver disease: a spectrum of clinical and pathological severity. *Gastroenterology* **116**, 1413-1419.
McGarry, J. D., Mannaerts, G. P. and Foster, D. W. (1977). A possible role for malonyl-CoA in the regulation of hepatic fatty acid oxidation and ketogenesis. *J. Clin. Invest.* **60**, 265-270.
Neuschwander-Tetri, B. A. and Caldwell, S. H. (2003). Nonalcoholic steatohepatitis: summary of an AASLD Single Topic Conference. *Hepatology* **37**, 1202-1219.
Powell, E. E., Cooksley, W. G., Hanson, R., Searle, J., Halliday, J. W. and Powell, L. W. (1990). The natural history of nonalcoholic steatohepatitis: a follow-up study of forty-two patients for up to 21 years. *Hepatology* **11**, 74-80.
Puri, P., Baillie, R. A., Wiest, M. M., Mirshahi, F., Choudhury, J., Cheung, O., Sargeant, C., Contos, M. J. and Sanyal, A. J. (2007). A lipidomic analysis of nonalcoholic fatty liver disease. *Hepatology* **46**, 1081-1090.
Ren, B., Thelen, A. P., Peters, J. M., Gonzalez, F. J. and Jump, D. B. (1997). Polyunsaturated fatty acid suppression of hepatic fatty acid synthase and S14 gene expression does not require peroxisome proliferator-activated receptor alpha. *J. Biol. Chem.* **272**, 26827-26832.
Robinson, J. S. and Mead, J. F. (1973). Lipid absorption and deposition in rainbow trout (Salmo gairdnerii). *Can. J. Biochem.* **51**, 1050-1058.
Sanyal, A. J. (2002). AGA technical review on nonalcoholic fatty liver disease. *Gastroenterology* **123**, 1705-1725.
Schaffner, F. and Thaler, H. (1986). Nonalcoholic fatty liver disease. *Prog. Liver Dis.* **8**, 283-298.
Sheridan, M. A. (1988). Lipid dynamics in fish: aspects of absorption, transportation, deposition and mobilization. *Comp. Biochem. Physiol. B* **90**, 679-690.
Sprecher, H. (1981). Biochemistry of essential fatty acids. *Prog. Lipid. Res.* **20**, 13-22.
Yamauchi, M., Kinoshita, M., Sasanuma, M., Tsuji, S., Terada, M., Morimyo, M. and Ishikawa, Y. (2000). Introduction of a foreign gene into medakafish using the particle gun method. *J. Exp. Zool.* **287**, 285-293.
Younossi, Z. M., Gramlich, T., Liu, Y. C., Matteoni, C., Petrelli, M., Goldblum, J., Rybicki, L. and McCullough, A. J. (1998). Nonalcoholic fatty liver disease: assessment of variability in pathologic interpretations. *Mod. Pathol.* **11**, 560-565.

Review

Iron regulation by hepatocytes and free radicals

Taro Takami[1] and Isao Sakaida[2,*]

[1]Division of Laboratory, Yamaguchi University Hospital, 1-1-1 Minami-kogushi, Ube, Yamaguchi 755-8505, Japan
[2]Department of Gastroenterology & Hepatology, Yamaguchi University Graduate School of Medicine, 1-1-1 Minami-kogushi, Ube, Yamaguchi 755-8505, Japan

(Received 29 June, 2010; Accepted 13 July, 2010; Published online 26 February, 2011)

Iron is an essential metallic microelement for life. However, iron overload is toxic. The liver serves an important role as a storehouse for iron in the body. About 20–25 mg of iron is required each day for hemoglobin synthesis. To maintain iron homeostasis, transferrin and transferrin receptors are primarily involved in the uptake of iron into hepatocytes, ferritin in its storage, and ferroportin in its export. Moreover, hepcidin controls ferroportin and plays a central role in the iron metabolism. Excess "free" reactive iron produces damaging free radicals via Fenton or Harber-Weiss reactions. Produced free radicals attack cellular proteins, lipids and nucleic acid. Several detoxification system and anti-oxidant defense mechanisms exist to prevent cellular damage by free radicals. Excessive free radicals can lead to hepatocellular damage, liver fibrosis, and hepatocarcinogenesis.

Key Words: **iron, hepatocyte, transferrin, hepcidin, free radicals**

Iron is the most abundant metallic microelement in the body, and it performs important actions in the body; being essential in hemoglobin synthesis for new erythrocytes (oxygen transport and delivery),[1] enzymes involving electron transport, iron-sulfur proteins,[2,3] and so on. The total amount of iron in the bodies of adult human males is about 5 g, of which approximately 65% is hemoglobin iron in erythrocytes.[1] The remainder is stored in ferritin in the liver and other organs.[4,5] Some iron is also present as myoglobin iron in muscles, heme iron in enzymes involved in respiration in all cells and drug metabolism. Daily food intake contains approximately 10 mg of iron, of which 1–2 mg is absorbed by the mucosa of the upper small intestine, bound to transferrin (Tf) in blood, and transported throughout the body as diferric transferrin (Fe_2-Tf). Iron homeostasis is maintained by the loss of about 1 mg of iron per day through the sloughing of intestinal mucosa and skin. However, 20–25 mg of iron is required each day for the hemoglobinization of new erythrocytes, for which iron in senescent erythrocytes, largely processed in reticuloendothelial cells, such as macrophages, is reused. As there appears to be no developed mechanism to evacuate accumulated iron from the body, excess iron intake can easily lead to iron overload in tissues, producing free radicals. This article provides an overview of iron metabolism in the liver, particularly in hepatocytes, and the production of free radicals caused by iron overload in the liver.

Iron in Hepatocytes

Iron absorbed from food in the upper small intestine is first transported to the liver via the portal vein. The liver not only stores iron, but also plays a crucial role in iron metabolism, such as in the production of Tf, iron carrier protein, and hepcidin known as a hormone that functions in the regulation of iron metabolism.

Mechanisms of iron transport into hepatocytes. Extracellular circulating iron in the plasma is present as soluble Tf-bound iron, and when there is excess iron, as non-transferrin-bound iron (NTBI), which is bound to serum proteins, such as albumin or citric acid.[6,7] Hepatocytes express both transferrin receptor (TfR) 1 and a homolog, TfR2.[8] Under neutral pH conditions, Tf binds two iron atoms with high affinity, and are circulated in the blood as Fe_2-Tf.[9] Known routes for the import of Fe_2-Tf into hepatocytes are via TfR1[10,11] and TfR2,[8] and a TfR-independent route.[12,13]

Fe_2-Tf binds with TfR1 on the cell membrane surface and forms a complex that is then taken up into hepatocytes by endocytosis.[14] Mice lacking TfR1 die during mid-gestation from reduction in erythrocyte sell size and hemoglobin content, an indication of its physiological essentiality.[15] TfR1 expression is controlled by the excess or deficiency of iron within cells, and is regulated by interactions between *trans*-acting iron regulatory proteins (IRP1 and IRP2) and multiple iron-responsive elements (IREs) present in the 3'-untranslated regions (UTRs) of TfR1 mRNA (The IRP-IRE regulatory system).[16–18] When there is insufficient iron, IRP binds with multiple IREs in the 3' UTR of TfR1 mRNA, and TfR1 protein levels increase via stabilization of the mRNA. In a state of excess iron, on the other hand, IRP is released from multiple IREs.[19] Thus, IRP acts as a sensor protein for intracellular iron and regulates the expression of IRE genes (Fig. 1A).

Once the Fe_2-Tf/TfR1 complex is endocytosed, the pH of endosomes is lowered to 5–6 by a proton pump ATPase.[20] The Fe_2-Tf bond is broken within acidic endosomes, and Fe^{3+} (ferric iron) is released within the endosome.[21] The free Fe^{3+} in endosomes then becomes Fe^{2+} (ferrous iron) by enzymes of the six-transmembrane epithelial antigen of the prostate (STEAP) family,[22,23] and subsequently transported to the cytoplasm by divalent metal transporter 1 (DMT1, also known as Nramp2 or DCT1), a member of the NRAMP (natural resistance-associated macrophage protein) family of metal iron transporters.[24,25] Much of the iron transported into the cytoplasm is employed in reactions for essential physiological reactions, such as mitochondrial adenosine triphosphate (ATP) generation, TCA cycle, and DNA damage repair.[26] Meanwhile, unused iron is stored in the iron-binding protein, ferritin. After dissociating from iron, apo-Tf and TfR1 return to the cell membrane surface, and are reused for further iron binding and uptake (Fig. 2 A–F).[21]

TfR2 was discovered in 1999 as a molecule highly homologous with the TfR1 gene,[8] and it was later shown that mutations in human TfR2 gene induced iron overload syndrome,[27] consistent with its important role in iron metabolism. TfR2 protein is distributed on the basolateral membrane of hepatocytes, and like the TfR1 protein, binds specifically to Tf.[28] IRE is not present in TfR2 mRNA; thus, its mRNA expression is almost completely unaffected by iron levels.[29] Nevertheless, when there is excess iron, Fe_2-Tf stabilizes the TfR2 protein, resulting in increased TfR2 protein levels.[30,31]

There are also reports of a route for the import of iron into hepatocytes that is not mediated by TfRs (Fig. 2G),[12,32] and the

*To whom corresnpondence should be addressed.
E-mail: sakaida@yamaguchi-u.ac.jp

doi: 10.3164/jcbn.10-76

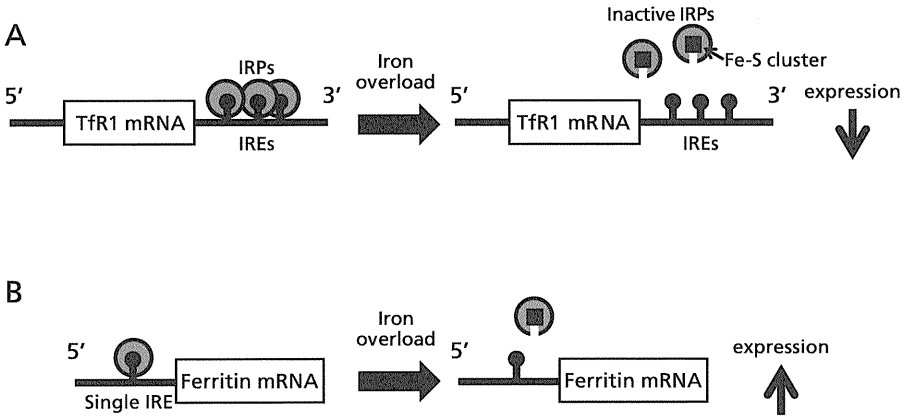

Fig. 1. The IRP-IRE regulatory system. A: Regulation of TfR1; at the high level of iron, the IRPs binding with multiple IREs in the 3' UTRs of TfR1 mRNA promotes TfR1 mRNA's translation via mRNA stabilization. B: Regulation of ferritin; the IRP binding with the single IRE in the 5' UTRs of ferritin mRNA blocks the translation of ferritin message. In iron overload, the IRP contained the Fe-S cluster cannot bind with the IRE in the 5' UTRs of ferritin mRNA, resulting in the increased translation of ferritin message.

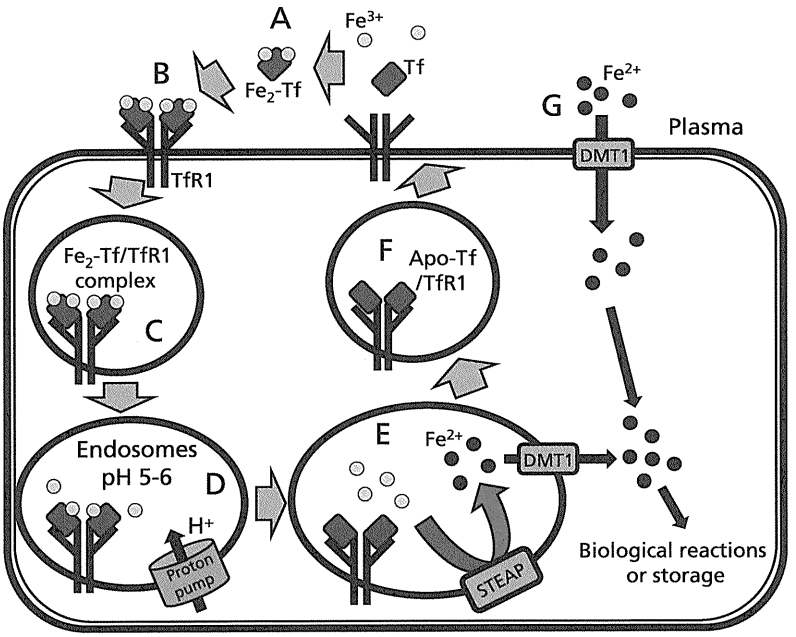

Fig. 2. Iron metabolism in hepatocytes. A–F: TfR-dependent route (the Tf cycle). A: Two ferric irons (Fe^{3+}) in the plasma bind to Tf with high affinity. B: Fe_2-Tf binds to TfR1 on the surface of hepatocytes. C: Fe_2-Tf/TfR1 complex is taken up into hepatocytes by endocytosis. D: The pH of endosomes is lowered to 5–6 by an action of proton pumps, and then Fe^{3+} is released at this acidic pH. E: Released Fe^{3+} becomes ferrous iron (Fe^{2+}) by the enzymes of STEAP family, and then Fe^{2+} moves across the endsomal membrane through the DMT1 transporter. F: Apo-Tf still binds to TfR1 at the lower pH of endosomes. Apo-Tf/TfR1 is returned to the surface of the hepatocyte for further iron binding and uptake. G: TfR-independent route. At the high level of iron in plasma, NTBI is reduced to Fe^{2+} by ferric reductase. Fe^{2+} is rapidly transported into the hepatocytes through DMT1.

involvement of DMT1[13] and the zinc transporter ZIP14 (Zrt-Irt-like protein 14)[33] molecules in the uptake of NTBI. In especially cardiomyocytes, it has been reported that L-type voltage-dependent calcium channels involved in the uptake of NTBI under iron overload condition.[34]

Iron storage in hepatocytes. Hepatocytes have a large capacity for iron storage. After iron's entering hepatocytes, the portion that is not used is stored in the cores of ferritin shells, in order to prevent subsequent toxicity.[35] When hepatocytes become heavily iron overload, an insoluble hemosiderin is derived from iron-rich ferritin.[5] Ferritin is an iron-storage protein comprising heavy (H) and light (L) subunits.[36] Fe^{2+} is oxidized to Fe^{3+} by ferroxidase in the H subunit, and then Fe^{3+} is stored in spaces within ferritin.[37] The synthesis of ferritin, like the TfR protein, is also regulated by IRP protein binding in the mRNA IRE region, and when the concentration of iron in cells increases, the amount of ferritin protein increases.[38,39] As some of the ferritin in the cell cytoplasm is secreted into extracellular medium, it can be measured in clinical tests to gauge the amount of iron stored in the body under non-inflammation conditions.

Regulation of iron export from hepatocytes. There is only 4 mg of iron in blood, and stored iron must be sent quickly

doi: 10.3164/jcbn.10-76

to the blood in order to maintain serum iron concentrations. Some kinds of cells, hepatocytes, intestinal epithelial cells and macrophages, have mechanisms to export iron. Iron is exported from cells by the ferroportin membrane protein (also known as IREG1 or MTP1),[40] and it is reported that in mice or Zebrafish lacking ferroportin, the supply of iron to the blood is almost entirely lost.[41] Iron sent into the blood is again transferred to Tf and is used in erythrocyte production in bone marrow. The expression of ferroportin is also regulated by the IRP-IRE regulatory system and hepcidin,[42] which is currently thought to play a central role in the iron metabolism.[43–46]

Hepcidin is synthesized in hepatocytes, secreted from hepatocytes, and excreted through the kidneys.[43,47] Hepcidin in its mature form is a 25-amino acid-peptide, hepcidin-25.[47] Hepcidin-25 binds with ferroportin and both are broken down in lysosomes by endocytosis.[46,48] Hepcidin-25 expression decreases and ferroportin iron export is promoted, when the body requires more serum iron, such as iron deficiency, hypoxia, and pregnancy.[47,49–50] However, in iron deficiency anemia in states of chronic inflammation, the supply of iron to the blood is inhibited by the reduced ferroportin function. It is thought that the inflammatory cytokine, interleukin-6 (IL-6), induces the expression of hepcidin-25 in hepatocytes, resulting in decreased ferroportin.[49,51] And when serum iron is not needed, hepcidin-25 expression increases and ferroportin is broken down, restricting the supply of iron.[47,49]

Iron Overload and Free Radicals

In healthy individuals, almost all of the iron in circulating blood is bound to Tf, while those in hepatocytes is bound to ferritin and isolated.[35] Ferritin has the capacity to hold 2,000–5,000 iron ions per a molecule, and as mentioned above, the amount of ferritin protein expressed increases with elevated intracellular levels of iron by the IRP-IRE regulatory system (Fig. 1B).[39] Ferritin can therefore handle even high amounts of iron imported into hepatocytes.[52] However, during iron overload, ferritin that is bound with iron undergoes denaturation in lysosomes to become hemosiderin, and Fe^{2+} is released from NTBI that is not bound to ferritin. When this occurs, Fe^{2+} reacts with hydrogen peroxide (H_2O_2) to generate hydroxyl radical ($^{\cdot}OH$) which have the highest toxicity among reactive oxygen species (ROS), via the Fenton reaction or Harber-Weiss reaction. And Fe^{2+} also reacts with lipid peroxides to generate lipid radicals. These radicals oxidize various cell components; including lipid membranes, proteins, and DNA, causing apoptosis or other cell damage.[53] The solubility of iron ions in the cytoplasm is very low; thus, they are assumed to be bound with other molecules, such as adenosine diphosphate (ADP), rather than be present as single ions. This notion is supported by the fact that administration of the iron chelating agent deferoxamine almost completely suppresses the cell damage from free radicals.[54,55] The risk of hepatocellular carcinoma (HCC) from hereditary hemochromatosis (HH) is about 200 times higher than that in healthy individuals. Interestingly, excess deposits of iron are also seen in hepatic tissues in chronic hepatitis C patients. It has been reported that chronic hepatitis C patients and hepatitis C virus (HCV) transgenic mice have lower levels of hepcidin, consistent with iron accumulation in the liver.[56–58] In such chronic hepatitis C patients, 8-hydroxydeoxy-guanosine (8-OHdG), an indicator of DNA damage by ROS, is significantly higher.[59] On the other hand, the rate of HCC from chronic hepatitis C patients treated with phlebotomy is significantly lower.[60] Moreover, it has been reported that the supplementation of exogenous antioxidants (vitamins A and E) reduced 8-OHdG levels in dietary iron overloaded rats.[61] These evidences *in vivo* and *in vitro* studies suggest that iron overload in the cytoplasm contributes, through the production of ROS, to both cellular damage and hepatocarcinogenesis.

Conclusions

Various molecules are involved in iron transport, storage, and export in hepatocytes, and because iron intake tends to be insufficient, despite being essential for life activity, systems for the reuse of iron have evolved. However, in states of iron overload from excess iron intake or chronic inflammation, harmful ROS are produced, and these may be able to cause hepatocellular damage and hepatocarcinogenesis.

Acknowledgment

This manuscript was partially supported by Grand-in-Aid for Scientific Research from the Japan Society for the Promotion of Science (No. 21790667).

Abbreviations

Tf	transferrin
Fe_2-Tf	diferric transferrin
NTBI	non-transferrin-bound iron
TfR	transferrin receptor
IRP	iron regulatory proteins
IRE	iron-responsive element
UTRs	untranslated regions
STEAP	six-transmembrane epithelial antigen of the prostate
DMT1	divalent metal transporter 1
NRAMP	natural resistance-associated macrophage protein
ATP	adenosine triphosphate
ZIP	Zrt-Irt-like protein
IL	interleukin
H_2O_2	hydrogen peroxide
ROS	reactive oxygen species
ADP	adenosine diphosphate
HCC	hepatocellular carcinoma
HH	hereditary hemochromatosis
HCV	hepatitis C virus
8-OHdG	8-hydroxydeoxy-guanosine

References

1 Wilson MT, Reeder BJ. Oxygen-binding haem proteins. *Exp Physiol* 2008; **93**: 128–132.
2 Rouault TA, Tong WH. Iron-sulphur cluster biogenesis and mitochondrial iron homeostasis. *Nat Rev Mol Cell Biol* 2005; **6**: 345–351.
3 Lill R, Mühlenhoff U. Iron-sulfur protein biogenesis in eukaryotes: components and mechanisms. *Annu Rev Cell Dev Biol* 2006; **22**: 457–486.
4 Harrison PM, Arosio P. The ferritins: molecular properties, iron storage function and cellular regulation. *Biochim Biophys Acta* 1996; **1275**: 161–203.
5 Koorts AM, Viljoen M. Ferritin and ferritin isoforms I: structure-function relationships, synthesis, degradation and secretion. *Arch Physiol Biochem* 2007; **113**: 30–54.
6 Silva AM, Hider RC. Influence of non-enzymatic post-translation modifications on the ability of human serum albumin to bind iron. Implications for non-transferrin-bound iron speciation. *Biochim Biophys Acta* 2009; **1794**: 1449–1458.
7 Silva AM, Kong X, Parkin MC, Cammack R, Hider RC. Iron(III) citrate speciation in aqueous solution. *Dalton Trans* 2009; **28**: 8616–8625.
8 Kawabata H, Yang R, Hirama T, and *et al.* Molecular cloning of transferrin receptor 2. A new member of the transferrin receptor-like family. *J Biol Chem* 1999; **274**: 20826–20832.
9 Sahlstedt L, von Bonsdorff L, Ebeling F, Ruutu T, Parkkinen J. Effective binding of free iron by a single intravenous dose of human apotransferrin in haematological stem cell transplant patients. *Br J Haematol* 2002; **119**: 547–553.
10 Aisen P. Transferrin receptor 1. *Int J Biochem Cell Biol* 2004; **36**: 2137–2143.
11 Hentze MW, Muckenthaler MU, Andrews NC. Balancing acts: molecular

control of mammalian iron metabolism. *Cell* 2004; **117**: 285–297.
12 Ikuta K, Zak O, Aisen P. Recycling, degradation and sensitivity to the synergistic anion of transferrin in the receptor-independent route of iron uptake by human hepatoma (HuH-7) cells. *Int J Biochem Cell Biol* 2004; **36**: 340–352.
13 Shindo M, Torimoto Y, Saito H, and *et al*. Functional role of DMT1 in transferrin-independent iron uptake by human hepatocyte and hepatocellular carcinoma cell, HLF. *Hepatol Res* 2006; **35**: 152–162.
14 Ciechanover A, Schwartz AL, Dautry-Varsat A, Lodish HF. Kinetics of internalization and recycling of transferrin and the transferrin receptor in a human hepatoma cell line. Effect of lysosomotropic agents. *J Biol Chem* 1983; **258**: 9681–9689.
15 Levy JE, Jin O, Fujiwara Y, Kuo F, Andrews NC. Transferrin receptor is necessary for development of erythrocytes and the nervous system. *Nat Genet* 1999; **21**: 396–399.
16 Pantopoulos K. Iron metabolism and the IRE/IRP regulatory system: an update. *Ann NY Acad Sci* 2004; **1012**: 1–13.
17 Rouault TA. The role of iron regulatory proteins in mammalian iron homeostasis and disease. *Nat Chem Biol* 2006; **2**: 406–414.
18 Cairo G, Recalcati S. Iron-regulatory proteins: molecular biology and pathophysiological implications. *Expert Rev Mol Med* 2007; **9**: 1–13.
19 Wang W, Di X, D'Agostino RB, Jr., Torti SV, Torti FM. Excess capacity of the iron regulatory protein system. *J Biol Chem* 2007; **282**: 24650–24659.
20 Klausner RD, Ashwell G, van Renswoude J, Harford JB, Bridges KR. Binding of apotransferrin to K562 cells: explanation of the transferrin cycle. *Proc Natl Acad Sci USA* 1983; **80**: 2263–2266.
21 Dautry-Varsat A, Ciechanover A, Lodish HF. pH and the recycling of transferrin during receptor-mediated endocytosis. *Proc Natl Acad Sci USA* 1983; **80**: 2258–2262.
22 Ohgami RS, Campagna DR, Greer EL, Antiochos B, McDonald A, Chen J. Identification of a ferrireductase required for efficient transferrin-dependent iron uptake in erythroid cells. *Nat Genet* 2005; **37**: 1264–1269.
23 Sendamarai AK, Ohgami RS, Fleming MD, Lawrence CM. Structure of the membrane proximal oxidoreductase domain of human Steap3, the dominant ferrireductase of the erythroid transferrin cycle. *Proc Natl Acad Sci USA* 2008; **105**: 7410–7415.
24 Fleming MD, Romano MA, Su MA, Garrick LM, Garrick MD, Andrews NC. Nramp2 is mutated in the anemic Belgrade (b) rat: evidence of a role for Nramp2 in endosomal iron transport. *Proc Natl Acad Sci USA* 1998; **95**: 1148–1153.
25 Ludwiczek S, Theurl I, Muckenthaler MU, and *et al*. Ca^{2+} channel blockers reverse iron overload by a new mechanism via divalent metal transporter-1. *Nat Med* 2007; **13**: 448–454.
26 Matsumoto Y, Zhang QM, Takao M, Yasui A, Yonei S. Escherichia coli Nth and human hNTH1 DNA glycosylases are involved in removal of 8-oxoguanine from 8-oxoguanine/guanine mispairs in DNA. *Nucleic Acids Res* 2001; **29**: 1975–1981.
27 Camaschella C, Roetto A, Cali A, and *et al*. The gene TFR2 is mutated in a new type of haemochromatosis mapping to 7q22. *Nat Genet* 2000; **25**: 14–15.
28 Merle U, Theilig F, Fein E, and *et al*. Localization of the iron-regulatory proteins hemojuvelin and transferrin receptor 2 to the basolateral membrane domain of hepatocytes. *Histochem Cell Biol* 2007; **127**: 221–226.
29 Kawabata H, Germain RS, Vuong PT, Nakamaki T, Said JW, Koeffler HP. Transferrin receptor 2-alpha supports cell growth both in iron-chelated cultured cells and *in vivo*. *J Biol Chem* 2000; **275**: 16618–16625.
30 Johnson MB, Enns CA. Diferric transferrin regulates transferrin receptor 2 protein stability. *Blood* 2004; **104**: 4287–4293.
31 Johnson MB, Chen J, Murchison N, Green FA, Enns CA. Transferrin receptor 2: evidence for ligand-induced stabilization and redirection to a recycling pathway. *Mol Biol Cell* 2007; **18**: 743–754.
32 Sturrock A, Alexander J, Lamb J, Craven CM, Kaplan J. Characterization of a transferrin-independent uptake system for iron in HeLa cells. *J Biol Chem* 1990; **265**: 3139–3145.
33 Liuzzi JP, Aydemir F, Nam H, Knutson MD, Cousins RJ. Zip14 (Slc39a14) mediates non-transferrin-bound iron uptake into cells. *Proc Natl Acad Sci USA* 2006; **103**: 13612–13617.
34 Oudit GY, Sun H, Trivieri MG, and *et al*. L-type Ca^{2+} channels provide a major pathway for iron entry into cardiomyocytes in iron-overload cardiomyopathy. *Nat Med* 2003; **9**: 1187–1194.
35 Munro HN. Iron regulation of ferritin gene expression. *J Cell Biochem* 1990; **44**: 107–115.
36 Boyd D, Jain SK, Crampton J, Barrett KJ, Drysdale J. Isolation and characterization of a cDNA clone for human ferritin heavy chain. *Proc Natl Acad Sci USA* 1984; **81**: 4751–4755.
37 Theil EC. Ferritin: at the crossroads of iron and oxygen metabolism. *J Nutr* 2003; **133**: 1549S–1553S.
38 Hentze MW, Caughman SW, Rouault TA, and *et al*. Identification of the iron-responsive element for the translational regulation of human ferritin mRNA. *Science* 1987; **238**: 1570–1573.
39 Hentze MW, Rouault TA, Caughman SW, and *et al*. A cis-acting element is necessary and sufficient for translational regulation of human ferritin expression in response to iron. *Proc Natl Acad Sci USA* 1987; **84**: 6730–6734.
40 Donovan PJ, Gearhart J. The end of the beginning for pluripotent stem cells. *Nature* 2001; **414**: 92–97.
41 Donovan A, Lima CA, Pinkus JL, Pinkus GS, Zon LI, Robine S. The iron exporter ferroportin/Slc40a1 is essential for iron homeostasis. *Cell Metab* 2005; **1**: 191–200.
42 Yeh KY, Yeh M, Glass J. Hepcidin regulation of ferroportin 1 expression in the liver and intestine of the rat. *Am J Physiol Gastrointest Liver Physiol* 2004; **286**: G385–G394.
43 Park CH, Valore EV, Waring AJ, Ganz T. Hepcidin, a urinary antimicrobial peptide synthesized in the liver. *J Biol Chem* 2001; **276**: 7806–7810.
44 Nicolas G, Bennoun M, Devaux I, and *et al*. Lack of hepcidin gene expression and severe tissue iron overload in upstream stimulatory factor 2 (USF2) knockout mice. *Proc Natl Acad Sci USA* 2001; **98**: 8780–8785.
45 Loréal O, Brissot P. Hepcidin: the Grail of iron metabolism. *Gastroenterol Clin Biol* 2002; **26**: 805–807.
46 Nemeth E, Tuttle MS, Powelson J, and *et al*. Hepcidin regulates cellular iron efflux by binding to ferroportin and inducing its internalization. *Science* 2004; **306**: 2090–2093.
47 Pigeon C, Ilyin G, Courselaud B, and *et al*. A new mouse liver-specific gene, encoding a protein homologous to human antimicrobial peptide hepcidin, is overexpressed during iron overload. *J Biol Chem* 2001; **276**: 7811–7819.
48 De Domenico I, Lo E, Ward DM, Kaplan J. Hepcidin-induced internalization of ferroportin requires binding and cooperative interaction with Jak2. *Proc Natl Acad Sci USA* 2009; **106**: 3800–3805.
49 Nicolas G, Chauvet C, Viatte L, and *et al*. The gene encoding the iron regulatory peptide hepcidin is regulated by anemia, hypoxia, and inflammation. *J Clin Invest* 2002; **110**: 1037–1044.
50 Millard KN, Frazer DM, Wilkins SJ, Anderson GJ. Changes in the expression of intestinal iron transport and hepatic regulatory molecules explain the enhanced iron absorption associated with pregnancy in the rat. *Gut* 2004; **53**: 655–660.
51 Nemeth E, Rivera S, Gabayan V, and *et al*. IL-6 mediates hypoferremia of inflammation by inducing the synthesis of the iron regulatory hormone hepcidin. *J Clin Invest* 2004; **113**: 1271–1276.
52 Miyazaki E, Kato J, Kobune M, and *et al*. Denatured H-ferritin subunit is a major constituent of haemosiderin in the liver of patients with iron overload. *Gut* 2002; **50**: 413–419.
53 Um HD, Orenstein JM, Wahl SM. Fas mediates apoptosis in human monocytes by a reactive oxygen intermediate dependent pathway. *J Immunol* 1996; **156**: 3469–3477.
54 Sakaida I, Kyle ME, Farber JL. Autophagic degradation of protein generates a pool of ferric iron required for the killing of cultured hepatocytes by an oxidative stress. *Mol Pharmacol* 1990; **37**: 435–442.
55 Sakaida I, Thomas AP, Farber JL. Increases in cytosolic calcium ion concentration can be dissociated from the killing of cultured hepatocytes by tert-butyl hydroperoxide. *J Biol Chem* 1991; **266**: 717–722.
56 Fujita N, Sugimoto R, Takeo M, and *et al*. Hepcidin expression in the liver: relatively low level in patients with chronic hepatitis C. *Mol Med* 2007; **13**: 97–104.
57 Nagashima M, Kudo M, Chung H, and *et al*. Regulatory failure of serum prohepcidin levels in patients with hepatitis C. *Hepatol Res* 2006; **36**: 288–293.
58 Nishina S, Hino K, Korenaga M, and *et al*. Hepatitis C virus-induced reactive oxygen species raise hepatic iron level in mice by reducing hepcidin transcription. *Gastroenterology* 2008; **134**: 226–238.
59 Kato J, Kobune M, Nakamura T, and *et al*. Normalization of elevated hepatic 8-hydroxy-2'-deoxyguanosine levels in chronic hepatitis C patients by phlebotomy and low iron diet. *Cancer Res* 2001; **61**: 8697–8702.
60 Kato J, Miyanishi K, Kobune M, and *et al*. Long-term phlebotomy with low-iron diet therapy lowers risk of development of hepatocellular carcinoma from chronic hepatitis C. *J Gastroenterol* 2007; **42**: 830–836.
61 Asare GA, Kew MC, Mossanda KS, Paterson AC, Siziba K, Kahler-Venter CP. Effects of exogenous antioxidants on dietary iron overload. *J Clin Biochem Nutr* 2009; **44**: 85–94.

doi: 10.3164/jcbn.10-76

Clinica Chimica Acta 412 (2011) 152–158

Contents lists available at ScienceDirect

Clinica Chimica Acta

journal homepage: www.elsevier.com/locate/clinchim

Efficient detection of hepatocellular carcinoma by a hybrid blood test of epigenetic and classical protein markers

Norio Iizuka [a,b], Masaaki Oka [a,*], Isao Sakaida [c], Toyoki Moribe [d], Toshiaki Miura [d], Naoki Kimura [d], Shigeru Tamatsukuri [d], Hideo Ishitsuka [d], Koichi Uchida [c], Shuji Terai [c], Satoyoshi Yamashita [e], Kiwamu Okita [e], Koichiro Sakata [f], Yoshiyasu Karino [g], Joji Toyota [g], Eiji Ando [h], Tatsuya Ide [h], Michio Sata [h], Ryoichi Tsunedomi [a], Masahito Tsutsui [a], Michihisa Iida [a], Yoshihiro Tokuhisa [a], Kazuhiko Sakamoto [a], Takao Tamesa [a], Yusuke Fujita [i], Yoshihiko Hamamoto [i]

[a] Departments of Surgery II Yamaguchi University Graduate School of Medicine, 1-1-1 Minami-Kogushi, Ube, Yamaguchi 755-8505, Japan
[b] Departments of Kampo Medicine Yamaguchi University Graduate School of Medicine, 1-1-1 Minami-Kogushi, Ube, Yamaguchi 755-8505, Japan
[c] Departments of Gastroenterology and Hepatology, Yamaguchi University Graduate School of Medicine, 1-1-1 Minami-Kogushi, Ube, Yamaguchi 755-8505, Japan
[d] Molecular Diagnostics R&D Department, Molecular Diagnostics Division, Roche Diagnostics K.K., 6-1, Shiba 2-chome, Minato-ku, Tokyo 105-0014, Japan
[e] Center of liver diseases, Social Insurance Shimonoseki Welfare Hospital, 3-3-8 Kamishinchi-cho, Shimonoseki, Yamaguchi, 750-0061, Japan
[f] Department of Surgery, Social Insurance Shimonoseki Welfare Hospital, 3-3-8 Kamishinchi-cho, Shimonoseki, Yamaguchi, 750-0061, Japan
[g] Department of Gastroenterology, Sapporo-Kosei General Hospital, Kita-3 Higashi-8-5, Chuo-ku, Sapporo, Hokkaido, 060-0033, Japan
[h] Division of Gastroenterology, Department of Medicine, Kurume University School of Medicine, 67 Asahi-machi, Kurume, Fukuoka, 830-0011 Japan
[i] Department of Computer Science and Systems Engineering, Faculty of Engineering, Yamaguchi University, 2-16-1 Tokiwadai, Ube, Yamaguchi 755-8611, Japan

ARTICLE INFO

Article history:
Received 28 April 2010
Received in revised form 21 September 2010
Accepted 22 September 2010
Available online 29 September 2010

Keywords:
HCV
HCC
Blood testing
Cell-free DNA
Hypermethylation
Quantitative MSP
Hybrid detector

ABSTRACT

Background: There are few blood tests for an efficient detection of hepatocellular carcinoma (HCC) associated with hepatitis C virus (HCV) infection.
Methods: The abilities of quantitative analyses of 7 genes hypermethylation in serum DNA, α-fetoprotein (AFP) and prothrombin-induced vitamin K absence II (PIVKA-II), and various combinations to detect HCC were evaluated in a training cohort of 164 HCV-infected patients (108 HCCs; 56 non-HCCs). An optimal hybrid detector, built using data for 2 methylated genes (*SPINT2* and *SRD5A2*), AFP, and PIVKA-II, achieved the most satisfactory ability to detect HCC in the training cohort. We evaluated the ability of the optimal hybrid detector to detect HCC in an independent validation cohort of 258 consecutive HCV-infected patients (112 HCCs; 146 non-HCCs) who were newly enrolled in 4 distinct institutes.
Results: In the validation cohort of 258 patients, accuracy, sensitivity, and specificity of the hybrid detector for detection of HCC were 81.4%, 73.2%, and 87.7%, respectively. Notably, even when detecting HCC ≤ 2 cm in diameter, the hybrid detector maintained markedly high abilities (84.6% accuracy, 72.2% sensitivity, 87.7% specificity). Youden's index (sensitivity + specificity − 1) for HCC ≤ 2 cm was 0.60, vastly much superior to the 0.39 for AFP at a cut-off value of 20 ng/ml and the 0.28 for PIVKA-II at a cut-off value of 40 mAU/ml.
Conclusions: These results show that the optimal hybrid blood detector can detect HCV-related HCC more accurately.

1. Introduction

For the last decade, evidence has been accumulating in various countries that hepatocellular carcinoma (HCC) is increasing [1–4] . This phenomenon can be explained partly by endemic infection with hepatitis C virus (HCV), one of the major etiological agents for development of HCC [5,6]. Despite the recent advent of treatment, HCC detected after the onset of symptoms shows a dismal prognosis (5-year survival, <10%) [5], indicating an urgent need for efficient detection systems to identify small, asymptomatic HCV-related HCC.

Current methods for diagnosis and screening of HCC include physical examination, various imaging techniques including ultrasonography (US), and measurements of serum α-fetoprotein (AFP) in certain risky populations, such as HCV-infected patients with liver cirrhosis (LC) [4,7]. AFP measurement for the detection of small HCCs (diameter ≤ 2 cm) has been questioned due to the low sensitivity and unstable cut-off values among studies or institutes [8]. The detection ability of US depends on examiner expertise, degree of patient obesity, presence of LC, and size of the liver tumor [9].

Epigenetic inactivation of transcription by aberrant methylation of CpG islands is a fundamental contributor to carcinogenesis [10].

* Corresponding author. Fax: +81 836 22 2262.
E-mail address: 2geka-1@po.cc.yamaguchi-u.ac.jp (M. Oka).

0009-8981/$ – see front matter © 2010 Elsevier B.V. All rights reserved.
doi:10.1016/j.cca.2010.09.028

Several genes reportedly undergo hypermethylation in the process of hepatocarcinogenesis [11–13]. Some studies have revealed the presence of circulating methylated genes in the bloodstream of HCC patients, but none has been applied to daily clinical use as a diagnostic tool [14,15].

In a genome-wide search using DNA array data, our recent study used a quantitative methylation-specific PCR (qMSP) technique to identify 2 unique genes (*BASP1* and *SRD5A2*) for which promoter methylation is specific for small HCC associated with HCV infection [16]. Moreover, we found that 5 known genes (*APC*, *RASSF1A*, *SPINT2*, *CCND2* and *CFTR*) were exclusively methylated in early HCC tissues [17].

Taken together, these prompted us to develop a serological parameter for the efficient detection of HCC associated with HCV. The present study therefore quantified levels of the 7 methylated marker genes [16,17], and classical tumor markers AFP and prothrombin-induced vitamin K absence II (PIVKA-II) in the blood of HCV-infected patients.

2. Materials and methods

2.1. Patients of the training cohort

In the present study, we utilized a training-validation approach [18,19] in which a hybrid detector was built *in silico* on the basis of information from only a training cohort, then the ability of this detector to identify HCC was evaluated in an independent validation cohort at multiple institutions (Fig. 1). Written informed consent was obtained from all patients. The study protocol was undertaken according to the REMARK criteria (http://www.cancerdiagnosis.nci.nih.gov/assessment/progress/remark.htm), and was approved by the Institutional Review Board for the Use of Human Subjects at Yamaguchi University School of Medicine and Review Boards for the Use of Human Subjects at another 3 institutes defined below.

Our training cohort (Table 1) included 164 patients positive for HCV antibody, all of whom were treated at Yamaguchi University Hospital between May 1998 and April 2006, and were subjected to analyses of AFP and PIVKA-II, routine radiography, US, computed tomography (CT), magnetic resonance imaging (MRI), and, if necessary, hepatic angiography, dynamic CT, or dynamic MRI before and after treatment. On the basis of those imaging techniques, 108 of the 164 patients were diagnosed with HCC. Subsequently, 95 of these 108 patients (88.0%) bearing HCC underwent hepatic surgery or biopsy; and all tumors from the 95 patients were pathologically confirmed as HCC. Moreover, none of the 108 HCC patients showed any other malignancies at enrollment. We confirmed that none of the remaining 56 patients developed HCC during the follow-up period of >2 years. On the basis of these findings, we classified the 108 patients with HCC and the remaining 56 patients into HCC and non-HCC groups, respectively (Table 1). Using the results of imaging techniques and pathological examinations, we judged that 79 of the 164 patients (48.2%) had liver cirrhosis (LC). As summarized in Table 1, we used the tumor-node-metastasis (TNM) staging system as revised by the Liver Cancer Study Group of Japan (LCSGJ) [20]. The present study defined HCC≤2 cm in diameter as "small HCC".

2.2. Patients of the validation cohort

Our validation cohort comprised 262 consecutive HCV-infected patients (Table 1) who were enrolled in 4 distinct institutes between

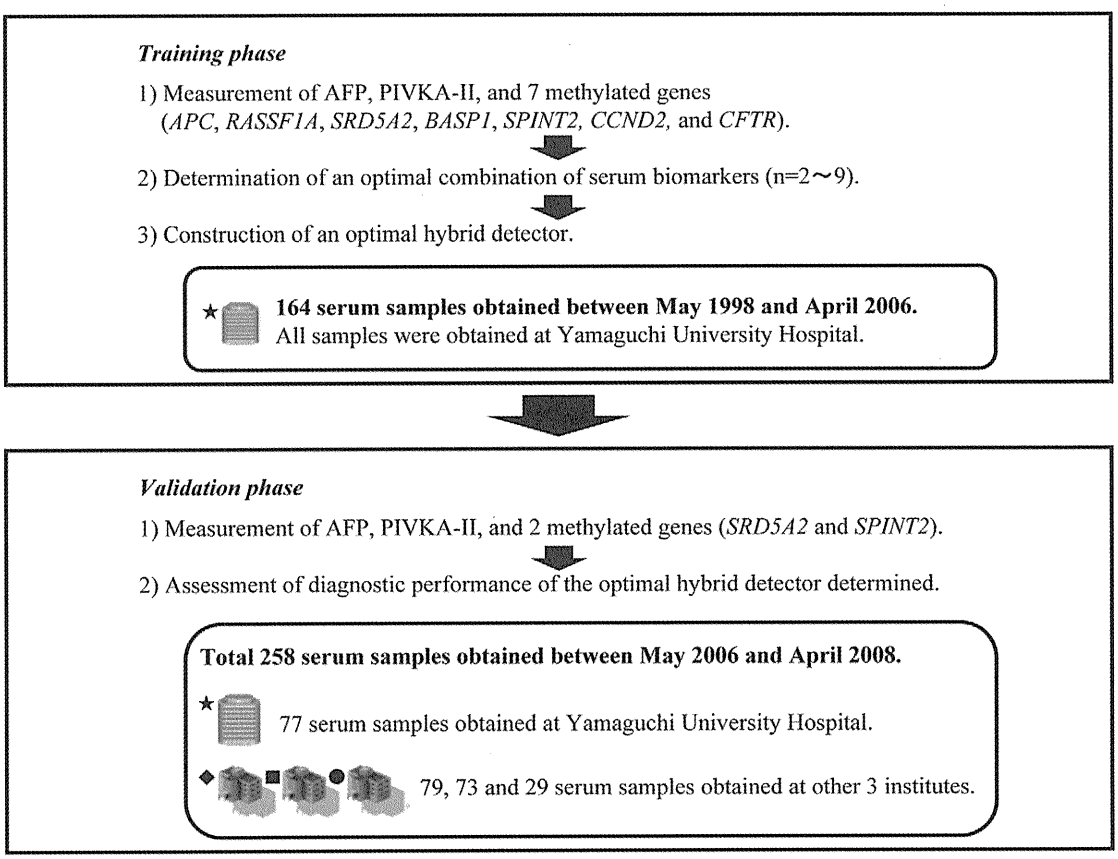

Fig. 1. Overview of the Training-Validation approach used for construction and evaluation of the hybrid detector for hepatocellular carcinoma.

Table 1
Patient characteristics in training and validation cohorts.

	HCC patients			Non-HCC patients		
	Training cohort (n = 108) (%)	Validation cohort (n = 112) (%)		Training cohort (n = 56) (%)	Validation cohort (n = 146) (%)	
Sex			$P = 0.004$[a]			$P = 0.062$[a]
Male	83 (76.8)	66 (58.9)		30 (53.6)	57 (39.0)	
Female	25 (23.2)	46 (41.1)		26 (46.4)	89 (61.0)	
Age (years) (mean ± SD)	66.6 ± 7.9	70.4 ± 8.0	$P < 0.0001$[b]	64.6 ± 7.8	64.6 ± 10.3	$P = 0.985$[b]
Serum ALT (U/L) (mean ± SD)	62.2 ± 65.4	55.9 ± 36.9	$P = 0.376$[b]	49.1 ± 34.0	51.0 ± 39.3	$P = 0.749$[b]
Platelet (10,000/mm^3) (mean ± SD)	12.3 ± 5.8	10.3 ± 5.4	$P = 0.008$[b]	14.5 ± 7.7	11.9 ± 6.1	$P = 0.012$[b]
Non-cancerous liver			$P = 0.028$[a]			$P < 0.0001$[a]
Chronic hepatitis	43 (39.8)	29 (25.9)		42 (75.0)	68 (46.6)	
Cirrhosis	65 (60.2)	83 (74.1)		14 (25.0)	78 (53.4)	
a feto-protein			$P = 0.618$[a]			$P = 0.041$[a]
<20 ng/ml	46 (42.6)	44 (39.3)		48 (85.7)	105 (71.9)	
>20 ng/ml	62 (57.4)	68 (60.7)		8 (14.3)	41 (28.1)	
PIVKA-II			$P = 0.207$[a]			$P = 0.088$[a]
<40 mAU/ml)	42 (38.9)	59 (52.7)		49 (87.5)	138 (94.5)	
>40 mAU/ml	66 (61.1)	53 (47.3)		7 (12.5)	8 (5.5)	
Tumor size			$P = 0.006$[a]			
<2.0 cm	22 (20.4)	36 (32.1)				
2.1–5.0 cm	62 (57.5)	67 (59.8)				
>5.0 cm	24 (22.1)	9 (8.1)				
Primary lesion			$P = 0.992$[a]			
Single	52 (48.1)	54 (48.2)				
Multiple	56 (51.9)	58 (51.8)				
Histological grading			$P = 0.900$[c]			
G1	21 (22.1)	12 (23.5)				
G2	63 (66.3)	32 (62.7)				
G3–G4	11 (11.6)	7 (13.8)				
Stage			$P = 0.077$[a]			
I	12 (11.1)	21 (18.7)				
II	42 (38.9)	32 (28.6)				
III	36 (33.3)	30 (26.8)				
IVA + IVB	18 (16.7)	29 (25.9)				

PIVKA-II, Prothrombin Induced Vitamin K Absence II.
[a] Chi-square test.
[b] Student's *t* test.
[c] Fisher exact test.

May 2006 and April 2008. Out of the 262 patients, 1 was excluded due to daily intake of warfarin, which may affect serum levels of PIVKA-II, and 3 were excluded because of small amounts of extracted cell-free DNA (cfDNA). Among the remaining 258 patients, 77 were treated at Yamaguchi University hospital, 73 at Shimonoseki Kohsei Hospital, 79 at Sapporo-Kosei General Hospital, and 29 at Kurume University Hospital. The detection program for HCC in individual institutes was performed according to the nationwide follow-up survey conducted by the LCSGJ [20] and/or the guidelines of the American Association for the Study of Liver Diseases (AASLD) [4]. On the basis of findings from multiple imaging modalities (US, CT, MRI, hepatic angiography, dynamic CT, and dynamic MRI), hepatologists from the individual institutes diagnosed 112 of the 258 patients (43.4%) as HCC. Among the 112 HCC patients, 52 were diagnosed at Yamaguchi University Hospital, 23 at Shimonoseki Kohsei Hospital, 24 at Sapporo-Kosei General Hospital, and 13 at Kurume University Hospital. Hepatic surgery or biopsy was subsequently performed for 51 of the 112 HCC patients (45.5%). All tumors, including 15 tumors ≤ 2 cm in diameter, from the 51 patients were pathologically confirmed as HCC, indicating the justification of our detection programs for HCC. Our follow-up program did not detect HCCs in any of the 146 patients initially defined as without HCC for 6 months after enrollment. Collectively, we categorized the 112 patients with HCC and the remaining 146 patients as HCC and non-HCC groups, respectively, in the validation cohort (Table 1).

2.3. Extraction and quantification of DNA in sera

Blood samples were collected from patients before treatment to measure methylated marker genes, AFP, PIVKA-II, alanine aminotransferase (ALT) and platelet count. We set a cut-off value of 20 ng/ml for AFP and a cut-off value of 40 mAU/ml for PIVKA-II for the discrimination of HCC, as these values have been shown to offer the highest diagnostic ability for HCV-related HCC and have been used most frequently in clinical practice [8,21]. As a source for methylation analysis, cfDNA was extracted from 1 ml of sera using a DNA Extractor SP Kit for Serum and Plasma (Wako Pure Chemical Industries, Osaka, Japan) according to the instructions from the manufacturer, and was quantified as described previously [22].

2.4. Measurement of methylated gene fragments circulating in sera

We performed qMSP assays for 2 novel methylated genes (*SRD5A2* and *BASP1*) and 5 other genes (*APC*, *RASSF1A*, *SPINT2*, *CCND2*, and *CFTR*), as described previously [16,17] (For gene selection, see supplementary material). In the training phase (Fig. 1), methylated forms of the 7 genes in patient sera were measured and calculated as methylated DNA amount in serum (picograms per 1 ml of serum). In the validation phase (Fig. 1), methylated forms of only *SRD5A2* and *SPINT2* in sera of patients were measured and calculated.

2.5. Development and evaluation of the hybrid detector

We used the Fisher linear classifier (FLC) [19] to construct a hybrid detector *in silico* where "HCC" and "non-HCC" are defined as groups A and B, respectively.

In FLC, the score is defined by

$$T(x) = f_A(x) - f_B(x)$$

where

$$f_A(x) = \frac{1}{2}(x-\hat{\mu}_A)^T\left[P(A)\hat{\Sigma}_A + P(B)\hat{\Sigma}_B\right]^{-1}(x-\hat{\mu}_A) + C(A).$$

$\hat{\mu}_A$ and $\hat{\Sigma}_A$ in $f_A(x)$ are the sample mean vector and sample covariance matrix for Group A, respectively, and $P(A)$ is a prior probability for Group A. $C(A)$–$C(B)$ in $T(x)$ is called Cut off. The value of Cut off can be optimized by minimizing the error rate estimated on the training samples. Then, FLC assigns a given x to be classified to Group A (i.e., HCC) if $T(x)<0$. FLC assigns a given x to be classified to Group B (i.e., non-HCC) if $T(x)>0$.

We input data for n markers ($n=2$-9) from the 164 training samples into FLC and evaluated the ability of constructed individual FLCs to detect HCC in the 164 training samples. Mean detection ability (i.e., sensitivity and accuracy) of top-10 combinations was maximal when the FLC was built using 4 markers (Fig. 2A). We next plotted specificity, sensitivity and diagnostic accuracy of each top-ranked combination of n markers ($n=2$–9). Likewise, a 4-marker combination (*SRD5A2*, *SPINT2*, AFP and PIVKA-II) achieved the highest sensitivity and accuracy among combinations of n markers (Fig. 2B).

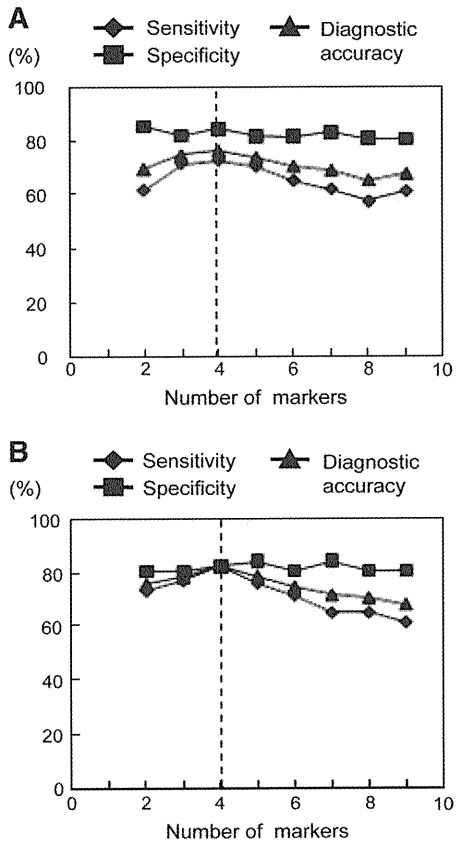

Fig. 2. Performances of markers in the training cohort. We input data for n markers ($n=2$–9) of the 164 training samples into Fisher linear classifier (FLC). This procedure was repeated for all combinations (from 9 C2 to 9 C9) of n markers and performances of the constructed individual FLCs were computed. Mean specificity, sensitivity and accuracy of the top 10 combinations of 2–7 markers and 9 combinations of 8 markers, and specificity, sensitivity and diagnostic accuracy for all 9 markers were plotted (A). Sensitivity and diagnostic accuracy were greater as the number of markers increased to 4; however, sensitivity and accuracy obtained using more than 4 markers were rather inferior to those obtained with 4 markers. We next plotted specificity, sensitivity and accuracy of each top-ranked combination of n markers ($n=2$–9) (B). A 4-marker combination of *SRD5A2*, *SPINT2*, AFP and PIVKA-II achieved the highest sensitivity and accuracy among combinations of n markers.

Collectively, using the optimal combination of 4 markers (*SRD5A2*, *SPINT2*, AFP and PIVKA-II), score was defined by

$$\begin{aligned} T(x) &= f_A(x) - f_B(x) \\ &= -136.28 \times (SRD5A2) - 1.78 \times (SPINT2) - 1.07 \times (\mathrm{AFP}) - 1.99 \\ &\quad \times (\mathrm{PIVKA\text{-}II}) + 131. \end{aligned}$$

where sample mean vectors and sample covariance matrices were estimated using the 164 training samples. Our hybrid detector classified samples as HCC or non-HCC for values of $T(x)<0$ and $T(x)>0$, respectively.

2.6. Perfectly blinded assessment of the validation cohort

To evaluate detection ability of the optimal hybrid detector established in the training cohort, we recruited another 258 patients with chronic HCV infection as the validation cohort. These patients were consecutively enrolled at each institute to maintain the independence of patient selection. In the present study, information regarding sample characteristics in the validation cohort was perfectly blinded for analysts of serum markers (TMo, TM, and NK) and bioinformaticians (YH and YF), who constructed a hybrid detector *in silico*.

2.7. Statistical analysis

The χ^2 test, Student's t test and Mann–Whitney U test were used to evaluate differences in tumor and patient characteristics between training and validation cohorts. Receiver operating characteristic (ROC) curve analysis was performed using SPSS for Windows version 11.0 J software (SPSS, Chicago, IL). Values of $P<0.05$ were considered significant.

3. Results

3.1. Patient characteristics

Significant differences in age and sex of HCC patients were seen between the training and validation cohorts ($P=0.004$ and $P<0.0001$, respectively; Table 1). HCC patients in the validation cohort showed significantly fewer platelets, higher frequency of coexisting LC, and smaller tumors compared to the training cohort ($P=0.008$, $P=0.028$ and $P=0.006$, respectively; Table 1). Non-HCC patients in the validation cohort showed significantly fewer platelets in peripheral blood, higher frequency of coexisting LC, and higher AFP levels than patients in the training cohort ($P=0.012$, $P<0.0001$, and $P=0.041$, respectively; Table 1).

3.2. Training phase

Among the 9 markers tested (Table 2), *SPINT2* and *SRD5A2* displayed high specificities (98.2% and 92.9%) but low sensitivities (35.2% and 8.3%) for HCC detection. *RASSF1A* for HCC detection had the highest sensitivity (83.3%), but showed a low specificity of 58.9%. No markers showed a Youden's index (sensitivity + specificity − 1) >0.6 for HCC detection in our training cohort, suggesting limitations to the single use of each marker. To improve this low detection ability, we attempted to build a hybrid detector system by combining data from several markers. We calculated all combinations of markers *in silico* and found that an optimal hybrid detector built using a 4-marker combination (*SRD5A2*, *SPINT2*, AFP and PIVKA-II) achieved the highest sensitivity, specificity and accuracy (82.4%, 82.1% and 82.3%, respectively) in the training cohort among all combinations of markers (Fig. 2B). This optimal hybrid detector showed a higher Youden's index (0.65) than any of the 9 markers tested (Table 2). We also

Table 2
Sensitivity, specificity, and accuracy of 9 biomarkers and the hybrid system for diagnosis of HCC or small HCC in the training cohort.

	Sensitivity (%)	Specificity (%)	Accuracy (%)	Youden's index
Methylation markers (cut-off value)				
BASP1 (0.2 pg per 1-ml serum)	62.0	78.6	71.2	0.41
CCND2 (0.2 pg per 1-ml serum)	64.8	42.9	60.3	0.08
APC (0.2 pg per 1-ml serum)	17.6	78.6	40.4	< 0
SPINT2[a] (0.2 pg per 1-ml serum)	35.2	98.2	59.6	0.33
SRD5A2[a] (0.2 pg per 1-ml serum)	8.3	92.9	39.1	0.01
CFTR (0.2 pg per 1-ml serum)	56.5	83.9	69.2	0.40
RASSF1A (0.2 pg per 1-ml serum)	83.3	58.9	72.4	0.42
Classical protein markers				
AFP[a] (20 ng/ml)	57.4	85.7	67.1	0.43
PIVKA-II[a] (40 mAU/ml)	60.2	89.3	70.1	0.50
Four-marker combination (cut-off value)				
Optimal hybrid system (0)	82.4	82.1	82.3	0.65

[a] Four markers used in the optimal hybrid system.

examined the methylation levels of the 7 methylated genes in the three groups consisting of patients who underwent previously or undergo currently therapies of interferon (IFN) combined with ribavirin, and patients who had no therapies of IFN combined with ribavirin. No significant differences in the methylation levels were found between ribavirin and non-rivavirin therapies (data not shown).

3.3. Validation phase

The ability of the optimal hybrid detector to detect HCC was evaluated using 258 sera from 258 HCV-infected patients in the validation cohort. Notably, sensitivity of PIVKA-II for HCC detection decreased from 60.2% in the training cohort to 51.8% in the validation cohort (Fig. 3A). The specificity of AFP for HCC detection decreased from 85.7% in the training cohort to 71.9% in the validation cohort (Fig. 3B). By contrast, the optimal hybrid detector maintained high sensitivity (73.2%), specificity (87.7%), and accuracy (81.4%) for HCC detection in the validation cohort (Fig. 3A–C). The positive predictive value and negative predictive value for HCC detection were 82.2% and 80.8%, respectively. Even for the detection of small HCC in the validation cohort, the optimal hybrid detector showed high sensitivity (72.2%), specificity (87.7%), and accuracy (84.6%) (Fig. 3A–C). As a result, the optimal hybrid detector for detection of HCC and/or small HCC maintained a Youden's index ≥ 0.6 throughout both training and validation cohorts (Fig. 3D). The optimal hybrid detector also judged all of 4 healthy peoples as non-HCC (data not shown).

The present study arbitrarily determined cut-off values of AFP and PIVKA-II, and directly applied these values to the validation cohort. We therefore had to compare the ability of the optimal hybrid detector with the maximal abilities of AFP and PIVKA-II alone in the validation samples. For this purpose, ROC curve analysis for the detection of HCC was performed for the validation cohort. AFP and PIVKA-II alone had areas under the ROC curve of 0.739 (95% confidence interval (CI), 0.678-0.799) and 0.794 (95% CI, 0.736-0.853), respectively, for HCC detection (Fig. 4). The optimal hybrid detector had a more global area under the ROC curve of 0.868 (95% CI, 0.822-0.913) compared to AFP and PIVKA-II, indicating that ability of the optimal hybrid detector was superior to the maximal abilities of AFP and PIVKA-II alone for detecting HCC in the validation cohort.

As summarized in Table 3, *SPINT2* and *SRD5A2* showed the highest accuracy in detecting non-HCC patients with chronic hepatitis or cirrhosis. AFP was most robust in detecting small HCC and PIVKA-II was most robust in detecting HCC > 2 cm in diameter. Apparently, the optimal hybrid detector possessed all of individual merits of the 2 methylated markers, AFP and PIVKA-II.

In the present study, the cost per each test of AFP, PIVKA-2, SRD5A2 and SPINT2 was $4, $17.6, $11.7 and $10.6, respectively. In the validation group, the specificity and diagnostic accuracy of AFP alone and the hybrid detector were 71.9% and 67.0%, and 87.7% and 81.4%, respectively (Fig. 3). Thus, AFP test plus $40 resulted in an increase of 15.8% and 14.4% of specificity and diagnostic accuracy, respectively. The areas under ROC curves of AFP alone and the hybrid detector were 0.739 and 0.868, respectively (Fig. 4). AFP test plus $40 resulted in an increase of 0.129 of the area.

In diagnosing HCC, the performance of the combined blood test of *SPINT2*, *SRD5A2*, AFP and PIVKA-2 was superior to that of the methylation test of 3 genes (*RASSF1*, *CCND2* and *SPINT2*) in HCC tissue developed in our previous study [17].

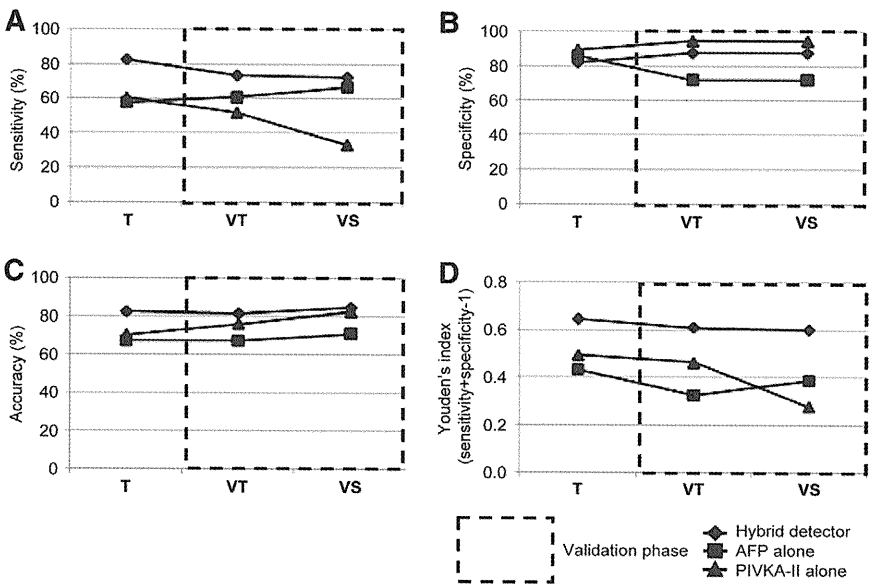

Fig. 3. Performances of the Optimal Hybrid detector (diamond), AFP (square), and PIVKA-II (triangle) in the validation cohort. The optimal hybrid detector showed the most robust performances for detection of HCC (A-D). T, training cohort of 108 HCC patients and 56 HCV carriers without HCC used for comparison with data from the validation cohort; VT, validation cohort of all 112 HCC patients and 146 HCV carriers without HCC; VS, validation cohort of 36 small HCC patients and 146 HCV carriers without HCC.

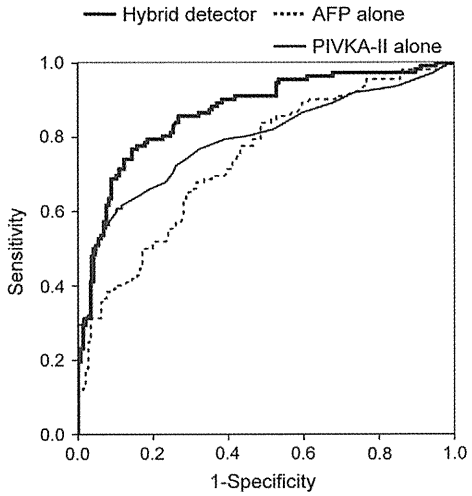

Fig. 4. Receiver operating characteristic curve analysis of the optimal hybrid detector, AFP, and PIVKA-II for the validation cohort.

4. Discussion

Many studies have evaluated AFP and PIVKA-II as detection tools for HCC, particularly small HCC. To the best of our knowledge, among studies using >100 samples, one study [23] showed a maximum sensitivity of 54.8%, but a specificity of only 49.1%, while another study [24] showed a maximum specificity of 71.0%, but a sensitivity of 25.0% in the ability of AFP to detect small HCC at a cut-off value of 20 ng/ml. A recent work by Marrero and colleagues showed that the optimal AFP cut-off value for diagnosis of HCC was 10.9 ng/ml leading to a sensitivity of 70% and a specificity of 82% [25]. However, the performance decreased to a sensitivity of 66% in diagnosing early HCC [25]. Another study showed that an AFP elevation (optimal cut-off value of 16 ng/ml) was indicative of HCC in non-infected patients, but not in HCV-infected patients [26]. For PIVKA-II, most studies with more than 100 samples showed sensitivities <40% for the detection of small HCC, with one study [27] reaching 53.5% sensitivity. Thus, reliance on the classical tumor markers AFP and PIVKA-II for the detection of HCC thus remains unsatisfactory, particularly given the low diagnostic powers and unstable cut-off values used between institutes [4,5,28]. To address these issues, we carefully conducted a multi-institutional study with multiple parameters, designed to develop a hybrid detector with more stable performance by searching for all combinations of marker candidates including methylated markers, as demonstrated previously by our laboratory [19]. The present study was also intended to minimize selection bias by using data collected consecutively only from HCV-infected patients [18,29]. We thus successfully developed a hybrid detector that accurately detected HCV-related HCC, particularly HCC≤2 cm in diameter, in a perfectly blinded manner in a multi-institutional large cohort.

Since the disclosure of epigenetic regulation in key genes, many studies [30–32] have shown the clinical efficacy of measuring promoter hypermethylation in various specimens such as tumor tissue, feces, and urine for determining the diagnosis and prognosis of cancer patients. Most studies measuring methylated DNA in the bloodstream of HCC patients have reported positive results, but almost all have been far from the setting of daily clinical use because of the insufficient performance due to the single use of a methylated marker gene [13–15,33]. We have provided herein the first evidence that a hybrid of methylation and classical protein markers has high potential for detecting HCV-related HCC in a blinded setting, opening new avenues toward the daily clinical application of methylated genes as tumor markers.

SPINT2 encodes hepatocyte growth factor (HGF) activator inhibitor type 2 (HAI-2) (http/www.ncbi.nlm.nih.gov/gene/10653), which regulates HGF activity. Epigenetic inactivation of *SPINT2* reportedly causes loss of tumor suppressor activity in renal cancer cells [34] and this gene is frequently hypermethylated in human HCC [12]. Consistent with those findings, our recent study [17] showed that *SPINT2* was frequently methylated in small HCC tissues, but unmethylated in non-HCC liver tissues, promising a high specificity for methylation patterns of *SPINT2* circulating in the bloodstream. *SRD5A2* encodes an enzyme that converts testosterone to the more active androgen dihydrotestosterone. Several polymorphisms in *SRD5A2* gene have been implicated as risk factors for prostate cancer [35]; however, how these polymorphisms act in the pathogenesis of HCC remains unclear.

We found that *RASSF1A*, *BASP1*, and *CCND2* offered more robust diagnostic performances than *SPINT2* and *SRD5A2* in the training phase. However, our *in silico* procedure predominantly selected the latter 2 genes for the optimal hybrid detector (Table 2). This result was consistent with our previous work [19,36], in which the diagnostic power of a detector built using several markers was independent of the ranking for diagnostic power of individual markers when combination was considered. In the validation phase, *SPINT2* and *SRD5A2* were very robust in detecting non-HCC patients, expectedly complementing the low detection ability of AFP and PIVKA-II (Table 3). Methylated *SPINT2* was also detectable in sera from 2 HCC cases negative for both AFP and PIVKA-II. This complementary effect is attributable to the absence of correlations between serum concentrations of AFP and PIVKA-II and those of methylated *SPINT2* and *SRD5A2* (data not shown). In addition to these independent expression patterns, our successful results might be partly attributable to a harmony of genetic features of *SPINT2* and *SRD5A2* and proteomic features of AFP and PIVKA-II. These features might maximize the synergistic power of the 4 markers.

The diagnostic accuracy of any test is related to the frequency of the underlying disease in the population being studied [4]. In the present study, many differences were seen between patient characteristics in the training and validation cohorts. In particular, the validation cohort included a significantly larger number of small HCCs than the training cohort ($P=0.006$; 36/112 vs. 22/108). This sample heterogeneity indeed resulted in decreased sensitivity of PIVKA-II alone and decreased specificity of AFP alone (Fig. 3A, B) for detecting small HCC in the validation cohort. The sensitivity and specificity of any test are inversely related. As a result, most studies have reported a Youden's index <0.5 for the diagnosis of small HCC. In contrast, our

Table 3
Diagnostic accuracy of markers and disease progression in the validation cohort.

Markers (cut-off value)	CH (%)	LC (%)	HCC≤2 cm (%)	HCC (2.1–5 cm) (%)	HCC>5 cm (%)	Total accuracy (%)
Optimal hybrid system (0)	65/68 (95.5)	63/78 (80.8)	26/36 (72.2)	48/67 (71.6)	8/9 (88.9)	210/258 (81.4)
SPINT2 (0.2 pg per 1-ml serum)	68/68 (100)	78/78 (100)	1/36 (2.78)	15/67 (22.4)	2/9 (22.2)	164/258 (63.6)
SRD5A2 (0.2 pg per 1-ml serum)	68/68 (100)	76/78 (97.4)	2/36 (5.56)	1/67 (1.50)	1/9 (11.1)	148/258 (57.4)
AFP (20 ng/ml)	60/68 (88.2)	45/78 (57.7)	24/36 (66.7)	37/67 (55.2)	7/9 (77.8)	173/258 (67.0)
PIVKA-II (40 mAU/ml)	67/68 (98.5)	71/78 (91.0)	12/36 (33.3)	40/67 (59.7)	7/9 (77.8)	197/258 (76.3)

CH, chronic hepatitis; LC, liver cirrhosis without HCC.
AFP, α-feto protein; PIVKA-II, prothrombin induced vitamin K Absence II.